INTERNATIONAL JOURNAL FOR NUMERICAL METHODS IN ENGINEERING
Int. J. Numer. Meth. Engng 2009; **77**:301–336
Published online 22 September 2008 in Wiley InterScience (www.interscience.wiley.com). DOI: 10.1002/nme.2403

Multi-actuated functionally graded piezoelectric micro-tools design: A multiphysics topology optimization approach

Ronny C. Carbonari[1], Emílio C. N. Silva[1] and Glaucio H. Paulino[2, *, †]

[1]*Department of Mechatronics and Mechanical Systems Engineering, Escola Politécnica da Universidade de São Paulo, Av. Prof. Mello Moraes, 2231, São Paulo, SP 05508-900, Brazil*
[2]*Newmark Laboratory, Department of Civil and Environmental Engineering, University of Illinois at Urbana-Champaign, 205 North Mathews Avenue, Urbana, IL 61801, U.S.A.*

SUMMARY

Micro-tools offer significant promise in a wide range of applications such as cell manipulation, micro-surgery, and micro/nanotechnology processes. Such special micro-tools consist of multi-flexible structures actuated by two or more piezoceramic devices that must generate output displacements and forces at different specified points of the domain and at different directions. The micro-tool structure acts as a mechanical transformer by amplifying and changing the direction of the piezoceramics output displacements. The design of these micro-tools involves minimization of the coupling among movements generated by various piezoceramics. *To obtain enhanced micro-tool performance, the concept of multifunctional and functionally graded materials is extended by tailoring elastic and piezoelectric properties of the piezoceramics while simultaneously optimizing the multi-flexible structural configuration using multiphysics topology optimization*. The design process considers the influence of piezoceramic property gradation and also its polarization sign. The method is implemented considering continuum material distribution with special interpolation of fictitious densities in the design domain. As examples, designs of a single piezoactuator, an XY nano-positioner actuated by two graded piezoceramics, and a micro-gripper actuated by three graded piezoceramics are considered. The results show that material gradation plays an important role to improve actuator performance, which may also lead to optimal displacements and coupling ratios with reduced amount of piezoelectric material. The present examples are limited to two-dimensional models because many of the applications for such micro-tools are planar devices. Copyright © 2008 John Wiley & Sons, Ltd.

Received 15 November 2006; Revised 30 April 2008; Accepted 16 May 2008

*Correspondence to: Glaucio H. Paulino, Newmark Laboratory, Department of Civil and Environmental Engineering, University of Illinois at Urbana-Champaign, 205 North Mathews Avenue, Urbana, IL 61801, U.S.A.
†E-mail: paulino@uiuc.edu, http://cee.uiuc.edu/paulino

Contract/grant sponsor: University of Illinois at Urbana-Champaign
Contract/grant sponsor: National Science Foundation; contract/grant number: CMS-0303492
Contract/grant sponsor: Conselho Nacional de Desenvolvimento Científico e Tecnológico (CNPq); contract/grant numbers: 140687-3, 476251/2004-4
Contract/grant sponsor: Fundação de Amparo a Pesquisa do Estado de São Paulo (FAPESP); contract/grant number: 2008/51070-0

Copyright © 2008 John Wiley & Sons, Ltd.

KEY WORDS: nano-positioners; micro-electro-mechanical systems (MEMs); functionally graded material (FGM); piezoelectric actuators; topology optimization; multiphysics

1. INTRODUCTION

Piezoelectric micro-tools offer significant promise in a wide range of applications involving nanopositioning and micromanipulation [1]. For instance, piezoelectric positioners are applied in atomic force microscopes and scanning tunneling microscopes for positioning the sample or the probe, respectively [2–4]; piezoelectric micro-grippers are applied to micromanipulation [5, 6], cell manipulation, and micro-surgery [7]. The micro-tools considered in this study essentially consist of multi-flexible structures actuated by two or more functionally graded piezoceramic devices that must generate different output displacements and forces at different specified points of the domain and at different directions. The multi-flexible structure acts as a *mechanical transformer* by amplifying and changing the direction of the piezoceramics output displacements [8]. Thus, the development of these piezoelectric micro-tools requires the design of actuated compliant mechanisms [9] that can accurately perform detailed specific movements. Although the design of such micro-tools is complicated due to the coupling between movements generated by various piezoceramics, it can be realized by means of topology optimization [10–12]. For instance, Figure 1 shows prototypes of a planar (*XY*) nanopositioner and a piezoelectric gripper. Here, topology optimization techniques are explored in conjunction with the concept of piezoceramic material gradation (to achieve enhanced micro-tool design), as discussed below.

Material gradation can be achieved by means of functionally graded materials (FGMs), which are special materials that possess continuously graded properties and are characterized by spatially varying microstructures created by nonuniform distributions of the reinforcement phase as well as by interchanging the role of reinforcement and matrix (base) materials in a continuous manner [13–15]. The smooth variation of properties may offer advantages such as local reduction of stress concentration and increased bonding strength [15].

Topology optimization is a powerful structural optimization method that seeks an optimal structural topology design by determining which points of space should be solid and which points should be void (i.e. no material) inside a given design domain [16]. However, the binary (0–1) design is an ill-posed problem and a typical way to seek a solution for topology optimization consists of relaxing the problem by defining a material model that allows for intermediate (composites)

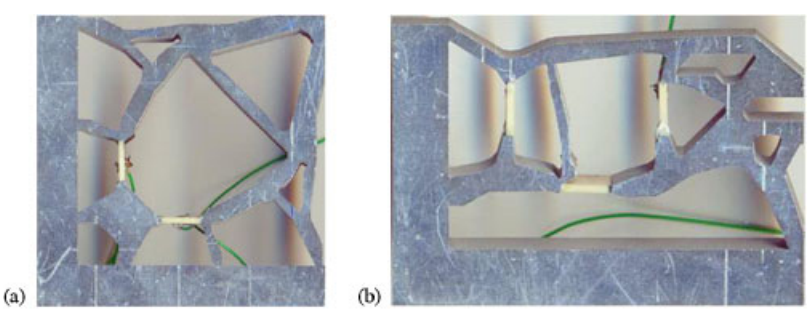

Figure 1. Micro-tools prototypes: (a) *XY* nanopositioner and (b) piezoelectric gripper.

Copyright © 2008 John Wiley & Sons, Ltd.

DOI: 10.1002/nme

property values [17]. In this sense, the relaxation yields a continuous material design problem that no longer involves a discernible connectivity. Typically, it is an improperly formulated (ill-posed) topology optimization problem for which no optimum solution exists (0–1 design). In general, a feasible topology solution can be obtained by applying penalization coefficients to the material model to recover the binary design (and thus, a discernible connectivity), together with some gradient control of material distribution, such as a filter [18].

The relaxed problem is related to the FGM design, which essentially seeks a continuous transition of material properties [13–15]. In contrast, although the 0–1 design problem needs complexity control (such as a filter) and does not admit intermediate values of design variables, the FGM design problem does not need complexity control and does admit solutions with intermediate values of the material field.

Owing to the attractive possibilities of tailoring material properties, some researchers have applied optimization methods to design FGMs. The study of Cho and Choi [19] presents a volume fraction optimization of each phase inside a domain considering reduction of thermal stress levels. The design of FGM structures with topology optimization has been considered by Turteltaub [20–22] focusing mainly on thermal and thermomechanical applications, including transient analysis, by defining the design variable in a piecewise fashion in the discretized domain. The application of a generic optimization method to tailor material property gradation has been proposed by Paulino and Silva [23] who applied topology optimization to solve the problem of maximum stiffness design.

Recently, the FGM concept has been explored in piezoelectric materials to improve their properties and to increase the lifetime of piezoelectric actuators [24]. Usually, elastic, piezoelectric, and dielectric properties are graded along the height of an FGM piezoceramic. Previous studies [24, 25] have shown that the gradation of piezoceramic properties can influence the performance of piezoactuators, such as generated output displacements. This suggests that optimization techniques can take advantage of the property gradation variation to improve the FGM piezoactuator performance. Thus, the objective of this work is to study the influence of piezoceramic property gradation and also its polarization sign variation in the design of multi-flexible micro-tool structures actuated by FGM piezoceramics using topology optimization. *Two design problems are considered simultaneously*: *the optimum design of the piezoceramic property gradation in the FGM piezoceramic domain*, *including polarization*, *and the design of the coupling structural topology.* Figure 2 illustrates the concept of multi-actuated flextensional FGM piezoelectric devices, as explored in the present study.

The optimization problem is posed as the design of a flexible structure, as well as each piezoceramic property gradation and polarization sign variation that maximizes different output

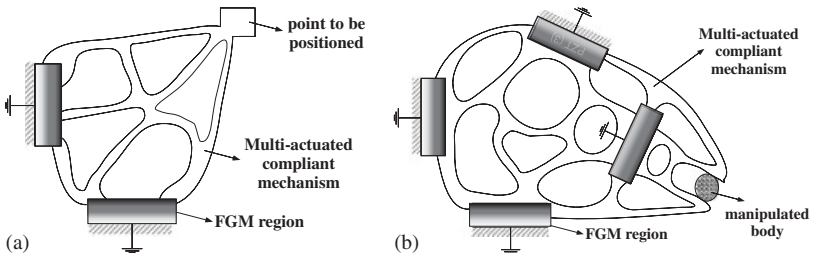

Figure 2. Concept of multi-actuated flextensional FGM piezoelectric devices: (a) FGM *XY* nanopositioner and (b) FGM piezoelectric gripper.

Copyright © 2008 John Wiley & Sons, Ltd.

DOI: 10.1002/nme

displacements or output forces at specified directions and points of the domain, in response to different excited piezoceramic portions while minimizing the effects of movement coupling [12]. For simplicity, the method is implemented based on the solid isotropic material with penalization (SIMP) model where fictitious densities are interpolated at each finite element (FE), providing a continuous material distribution in the domain. The optimization algorithm employed is based on sequential linear programming (SLP) [26, 27]. Other material models or optimization algorithms may also be explored. The examples provided include designs of a single piezoactuator, a planar (XY) nano-positioner actuated by two FGM piezoceramics, and a micro-gripper actuated by three FGM piezoceramics. The resulting designs are compared with designs considering conventional homogeneous piezoceramics.

Our approach to treat functionally graded piezoceramic materials requires three design variables: ρ_1 (design variable associated to material distribution in the structural region), ρ_2 (design variable associated to piezoceramic material distribution), and ρ_3 (binary design variable associated to polarization sign). Previous study in this area [12] did not account for any material gradation effects and considered 'fixed' piezoceramics. Thus, the main contributions of this study are as follows:

- treatment of functionally graded piezoceramic materials (FGMs);
- progressive change of electrode position induced by the piezoceramic gradation;
- material optimization within the piezoceramic domain;
- optimization of polarization sign;
- consideration of material gradation and change of polarization to explore bending in the piezoceramic (the resulting stress levels are low compared with stresses generated by the usual range of applied electrical field).

This paper is organized as follows. In Section 2, a brief introduction about the FE formulation for piezoelectricity considering the FGM concept is presented. In Section 3, the continuous topology optimization method, the underlining material model, and the formulation of the topology optimization problem applied to piezoelectric micro-tool design considering FGM piezoceramics are described. In Section 4, some aspects of the numerical implementation are discussed. In Section 5, an account of sensitivity analysis is given using the adjoint method. In Section 6, a technique for explicit control of material gradation through projection is presented. In Section 7, numerical examples are given including FGM piezoelectric micro-tool designs. In this study, the dielectric properties are not altered in the piezoceramic domain. Finally, in Section 8, conclusions are inferred.

2. FE FGM PIEZOELECTRIC MODELING

The micro-tools considered here operate in quasi-static or low-frequency applications (inertia effects are neglected). The weak formulation of the equilibrium equations of the piezoelectric medium considering linear piezoelectricity is well developed and it is given by [28]

$$\begin{aligned} &\int_\Omega \boldsymbol{\epsilon}(\mathbf{u})^{\mathrm{t}}\mathbf{c}^{\mathrm{E}}\boldsymbol{\epsilon}(\mathbf{v})\,\mathrm{d}\Omega+\int_\Omega(\nabla\phi)^{\mathrm{t}}\mathbf{e}^{\mathrm{t}}\boldsymbol{\epsilon}(\mathbf{v})\,\mathrm{d}\Omega=\int_{\Gamma_{\mathbf{t}}}\mathbf{t}\cdot\mathbf{v}\,\mathrm{d}\Gamma \\ &\int_\Omega \boldsymbol{\epsilon}(\mathbf{u})^{\mathrm{t}}\,\mathbf{e}\nabla\varphi\,\mathrm{d}\Omega-\int_\Omega(\nabla\phi)^{\mathrm{t}}\boldsymbol{\varepsilon}^{\mathrm{S}}\nabla\varphi\,\mathrm{d}\Omega=\int_{\Gamma_d}\mathrm{d}\varphi\,\mathrm{d}\Gamma \end{aligned} \quad \text{for } \mathbf{u},\ \phi\in V \text{ and } \forall\mathbf{v},\ \forall\varphi\in V \tag{1}$$

Copyright © 2008 John Wiley & Sons, Ltd.

DOI: 10.1002/nme

where

$$\mathbf{t}=\mathbf{T}\cdot\mathbf{n}, \quad d=\mathbf{D}\cdot\mathbf{n} \tag{2}$$

T, **D** are the stress tensor and the electrical displacement vector, respectively, **n** is the normal vector to the surface, and

$$V=\{\mathbf{v}=v_i\bar{\mathbf{e}}_i, \varphi \text{ with } \mathbf{v}=0 \text{ on } \Gamma_{\mathbf{u}} \text{ and } \varphi=0 \text{ on } \Gamma_\phi,\ i=1 \text{ or } 3\} \tag{3}$$

Ω is the domain of the piezoelectric medium (but it may also contain non-piezoelectric materials), ∇ is the gradient operator, and $\mathbf{c}^{\mathrm{E}}$, **e**, and $\boldsymbol{\varepsilon}^{\mathrm{S}}$ denote the elastic, piezoelectric, and dielectric properties, respectively, of the medium. The superscript 't' denotes transpose, **v** and φ are virtual displacements and electric potential, respectively, **u** is the displacement field, **t** is the mechanical traction, d is the electrical charge, and ϕ is the electric potential in the piezoelectric medium. The index i assumes value either 1 or 3 because the problem is considered in the 1–3 plane. The piezoceramic is polarized in the local 3 direction, and the strain–displacement relation is given by

$$\varepsilon_{ij}(\mathbf{u})=\frac{1}{2}\left(\frac{\partial u_i}{\partial x_j}+\frac{\partial u_j}{\partial x_i}\right) \tag{4}$$

The linear FE matrix formulation of the equilibrium equations for the piezoelectric medium is given by [28]

$$\begin{bmatrix}\mathbf{K}_{uu} & \mathbf{K}_{u\phi}\\ \mathbf{K}_{u\phi}^{\mathrm{t}} & -\mathbf{K}_{\phi\phi}\end{bmatrix}\begin{Bmatrix}\mathbf{U}\\ \boldsymbol{\Phi}\end{Bmatrix}=\begin{Bmatrix}\mathbf{F}\\ \mathbf{Q}\end{Bmatrix}\Longrightarrow[\mathscr{K}]\{\mathscr{U}\}=\{\mathscr{Q}\} \tag{5}$$

where $\mathbf{K}_{uu}$, $\mathbf{K}_{u\phi}$, and $\mathbf{K}_{\phi\phi}$ denote the stiffness, piezoelectric, and dielectric matrices, respectively, and **F**, **Q**, **U**, and $\boldsymbol{\Phi}$ are the nodal mechanical force, nodal electrical charge, nodal displacements, and nodal electric potential vectors, respectively [28].

In the case of FGM piezoceramics, the properties change continuously inside the piezoceramic domain, which means that they can be described by some continuous function of position **x** in the piezoceramic domain, that is

$$\mathbf{c}^{\mathrm{E}}=\mathbf{c}^{\mathrm{E}}(\mathbf{x}), \quad \mathbf{e}=\mathbf{e}(\mathbf{x}), \quad \boldsymbol{\varepsilon}^{\mathrm{S}}=\boldsymbol{\varepsilon}^{\mathrm{S}}(\mathbf{x}) \tag{6}$$

From the mathematical definitions of $\mathbf{K}_{\mathbf{uu}}$, $\mathbf{K}_{\mathbf{u}\phi}$, and $\mathbf{K}_{\phi\phi}$, these material properties should remain inside the matrices integrals and be integrated together by using the graded FE concept [29] where properties are continuously interpolated inside each FE based on property values at each FE node. An attempt to approximate the continuous change of material properties by a stepwise function where a property value is assigned for each finite element may result in less accurate results with undesirable discontinuities of the stress and strain fields (see, for example, Reference [29]).

When a non-piezoelectric conductor material and a piezoceramic material are distributed in the piezoceramic domain, the electrode positions are not known '*a priori*,' as discussed ahead. Therefore, the electrical excitation is given by an applied electric field [30] ($\nabla\phi=$constant), and

Copyright © 2008 John Wiley & Sons, Ltd.

DOI: 10.1002/nme

thus, Equation (1) becomes

$$\begin{aligned} \int_\Omega \boldsymbol{\epsilon}(\mathbf{u})^{\mathrm{t}}\mathbf{c}^{\mathrm{E}}\boldsymbol{\epsilon}(\mathbf{v})\,\mathrm{d}\Omega &= \int_{\Gamma_{\mathbf{t}}} \mathbf{t}\cdot\mathbf{v}\,\mathrm{d}\Gamma - \int_\Omega (\boldsymbol{\nabla}\phi)^{\mathrm{t}}\mathbf{e}^{\mathrm{t}}\boldsymbol{\epsilon}(\mathbf{v})\,\mathrm{d}\Omega \\ \int_\Omega \boldsymbol{\epsilon}(\mathbf{u})^{\mathrm{t}}\mathbf{e}\nabla\varphi\,\mathrm{d}\Omega &= \int_\Omega (\boldsymbol{\nabla}\phi)^{\mathrm{t}}\boldsymbol{\varepsilon}^{\mathrm{S}}\boldsymbol{\nabla}\varphi\,\mathrm{d}\Omega + \int_{\Gamma_d} \mathrm{d}\varphi\,\mathrm{d}\Gamma \end{aligned} \quad \text{for } \mathbf{u},\ \phi\in V \text{ and } \forall\mathbf{v},\ \forall\varphi\in V \tag{7}$$

In this case, all electrical degrees of freedom are specified in the FE problem, and Equation (5) becomes

$$\begin{aligned} [\mathbf{K}_{uu}]\{\mathbf{U}\} &= \{\mathbf{F}\} - [\mathbf{K}_{u\phi}]\{\boldsymbol{\Phi}\} \\ [\mathbf{K}_{u\phi}^{\mathrm{t}}]\{\mathbf{U}\} &= \{\mathbf{Q}\} + [\mathbf{K}_{\phi\phi}]\{\boldsymbol{\Phi}\} \end{aligned} \tag{8}$$

as $\{\boldsymbol{\Phi}\}$ is specified. Accordingly, the mechanical and electrical problems are decoupled, and only the upper problem of Equation (8) needs to be directly solved. Essentially, the optimization problem is based on the mechanical problem. As a consequence, the dielectric properties do not influence the design.

3. DESIGN PROBLEM FORMULATION

The basic topology optimization framework used in this study is described in detail by Carbonari *et al.* [12] and it is based on the continuous topology optimization concept where a continuum distribution of the design variable inside the finite element is considered through interpolation using a continuous function. In this case, the design variables are defined for each element node [31] instead of each finite element as usual [18]. This formulation, known as 'continuous approximation of material distribution' (CAMD) [31, 32] appears to be robust for designing the piezoelectric micro-tools [12] of interest in this study. As indicated in the Introduction, the material model is based on the SIMP [18] method combined with the CAMD approach and states that at each point of the domain, the local stiffness of the mixture $\mathbf{C}^{\mathrm{H}}$ as

$$\mathbf{C}^{\mathrm{H}} = \rho_1^p \mathbf{C}_0 \tag{9}$$

where $\mathbf{C}^{\mathrm{H}}$ and $\mathbf{C}_0$ are the elastic properties of the mixture and basic material that is distributed in the domain, respectively, ρ_1 is a pseudo-density describing the amount of material at each point of the design domain, which can assume values between 0 and 1, and $p\in[1,3]$ is a penalization factor to recover the discrete design. For ρ_1 equal to 0 the material corresponds to void, and for ρ_1 equal to 1 the material corresponds to solid material. For a domain discretized into finite elements with continuum distribution of design variable, Equation (9) is considered for each element node, and the material property (e.g. Young's modulus) inside each finite element is given by a function $\rho_1(\mathbf{x})$, where $\mathbf{x}$ denotes the Cartesian coordinates. This formulation leads to a continuous distribution of material in the design domain (instead of the traditional piecewise material distribution applied to previous formulations of topology optimization), and it is also compatible with the FGM concept considered in the piezoceramic domain.

Because the objective of this study also consists of optimizing the material gradation in the piezoceramic domain, an additional material model must be defined for this domain. Therefore, a new design variable ρ_2 is introduced to describe the type of piezoelectric material. In addition,

Copyright © 2008 John Wiley & Sons, Ltd.

DOI: 10.1002/nme

the polarization sign in the piezoelectric domain must be taken into account to increase design flexibility. This can be achieved by changing the sign of the piezoelectric property **e**. Thus, a new design variable ρ_3 is introduced, which describes the polarization of the piezoelectric material [33]. As shown later, it is very important that the polarization be part of the optimization process—this improves significantly the design and performance of the final actuator. The following material models are introduced based on an extension of the traditional SIMP model [18]:

$$\mathbf{C}^{\mathrm{H}} = \rho_2 \mathbf{C}_1 + (1-\rho_2)\mathbf{C}_2 \tag{10}$$

$$\mathbf{e}^{\mathrm{H}} = (2\rho_3 - 1)^{p_e}[\rho_2 \mathbf{e}_1 + (1-\rho_2)\mathbf{e}_2] \tag{11}$$

where ρ_2, a pseudo-density function defined at each point of the domain, is described as follows:

- $\rho_2 = 1.0$ denotes piezoelectric material *type 1*;
- $\rho_2 = 0.0$ denotes piezoelectric material *type 2*.

The design variables can assume different values at each finite element node. The tensors $\mathbf{C}^{\mathrm{H}}$ and $\mathbf{e}^{\mathrm{H}}$ are stiffness and piezoelectric properties, respectively. The tensors $\mathbf{C}_j$ and $\mathbf{e}_j$ are related to the stiffness and piezoelectric properties for piezoelectric material type j ($j = 1, 2$), respectively. These are the properties of basic materials that are distributed in the piezoceramic domain.

The specific material model described by Equation (9) allows material change from void to non-piezoelectric material (e.g. Aluminum), while the material model described by Equations (10) and (11) allows change from material *type 1* to *type 2* (one of these materials maybe Aluminum). Note that these material models are independent from each other and are defined in independent design domains. Thus, the material model described by Equation (9) and the material model described by Equations (10) and (11) are uncoupled. The main motivation to formulate problem in this manner is to achieve designs that are more realistic in terms of manufacturing. For instance, the Aluminum structure can be (and has been) fabricated using electrical discharge machining, as illustrated by Figure 1, while the graded piezoceramic could be fabricated using a processing technique such as spark plasma sintering [15].

The material model described by Equations (10) and (11) does not allow material change involving void phase, material *type 1* and material *type 2*. Of course, we expect that by distributing 3 phases (rather than 2), different topologies will be obtained. Actually, inclusion of void phase is not within the scope of the present study. Ongoing study by the authors considers material change from void and FGM made of materials *type 1* and *type 2* following the idea of coupling the material model given by Equation (9) and the material model given by Equations (10) and (11). Preliminary results can be found in Reference [34]. Moreover, Carbonari *et al.* [35] discuss the distribution of void, material *type 1* and *type 2*; however, the FGM concept has not been explored.

The dielectric properties are not considered because a constant electric field is applied to the design domain as electrical excitation and, as explained later (Section 4), this approach decouples the electrical and mechanical problems eliminating the influence of dielectric properties in the optimization problem. Eventually, the piezoelectric material *type 2* can be substituted by the flexible structure material (non-piezoelectric material, such as Aluminum, for example), and in this case $\mathbf{e}_2 = \mathbf{0}$. Analogous to the material model described by Equation (9), ρ_2 does have a continuous distribution along the piezoceramic design domain, that is, $\rho_2 = \rho_2(\mathbf{x})$, and so does the material properties. For a discretized domain into finite elements, ρ_2 and Equations (10) and (11) are considered for each finite element node. Thus, by finding the nodal values of the unknown ρ_2 function, we are indirectly finding the optimum material distribution functions, which are described by Equation (6).

Copyright © 2008 John Wiley & Sons, Ltd.

DOI: 10.1002/nme

The design variable ρ_3 is related to the polarization sign in the piezoceramic domain. Its value should tend to zero or unity, indicating that the polarization is either negative or positive, respectively. The penalization factor p_e is an odd number that is applied to avoid intermediate values of ρ_3 as we are interested only in positive or negative polarization signs. Thus, this material model allows the algorithm not only to optimize the material distribution but also to choose a suitable polarization (either positive or negative) at each point.

Essentially, a piezoelectric multi-actuator consists of a coupling structure actuated by two or more piezoceramics [8] where each piezoceramic is responsible for actuating a specific multi-actuator movement. In addition, there is a coupling among actuated displacements due to the fact that it is a flexible structure. Thus, when a piezoceramic is excited to generate a desired displacement, other undesired displacements may also be generated. These undesired displacements can be reduced by decoupling as much as possible the actuated and undesired displacements. Figure 3 shows an example of a coupling structure multi-actuated by piezoceramics.

The electrical excitation approach is discussed next. When the distribution of a non-piezoelectric conductor material and a piezoceramic material is considered in the piezoceramic domain, the electrode positions are not known '*a priori*.' To circumvent this problem, an electric field is applied as electrical excitation [30]. If two piezoelectric materials are considered, then the electrode positions are known and an electric field excitation can be achieved by applying an electric voltage to the electrodes whose positions are known and correspond to the boundary of the piezoceramic domain.

Therefore, in the formulation of the piezoelectric multi-actuator design optimization, the objective is to design a device such that when each piezoceramic is actuated, it generates an output displacement at a specified point and direction, which has minimum coupling with displacements generated by other piezoceramics at other points and directions. Thus, this design problem is related

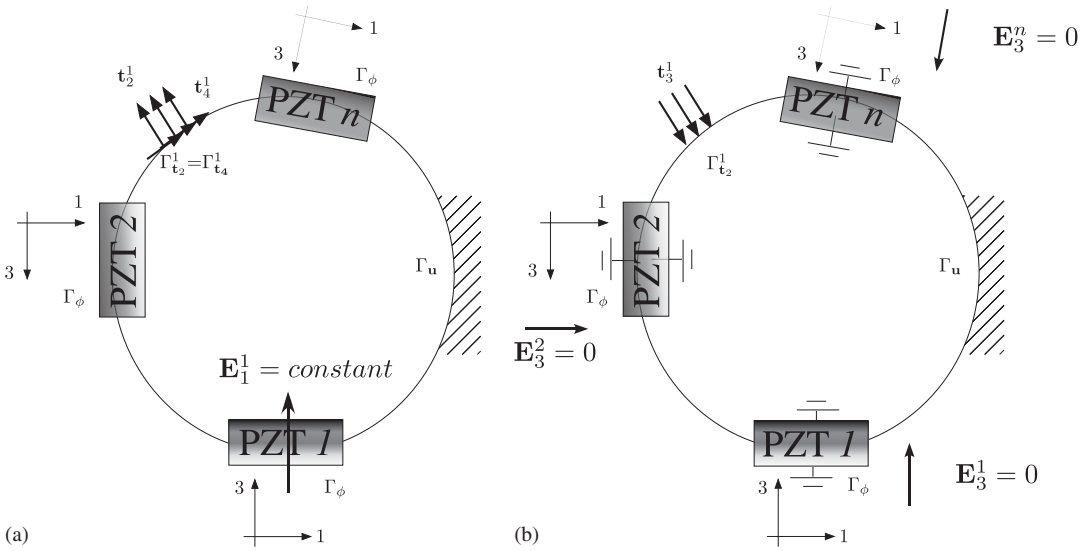

Figure 3. Coupling structure multi-actuated by FGM piezoceramics. Here, $\mathbf{E}_i^j = -\nabla\phi_i$ denotes the electrical field associated with load case i applied to piezoceramic j. Load cases for calculation of (a) mean transduction and coupling constraint function (for first piezoceramic only, i.e. PZT*1*) and (b) mean compliance.

Copyright © 2008 John Wiley & Sons, Ltd.

DOI: 10.1002/nme

to flexible structures design theory considering multi-flexibility [36]. The objective function is defined in terms of a combination of output displacements generated for a specified applied electric field to each piezoceramic, and it must also minimize the coupling among displacements, which can be achieved by including coupling constraints. The objective function is composed of three types of functions: *mean transduction*, *mean compliance*, and *coupling constraint* terms. Their mathematical expressions are given by Carbonari *et al.* [12]; however, they are also presented here considering the electric field excitation.

The *mean transduction* ($L_2^i(\mathbf{u}_1^i, \phi_1^i)$) concept is related to the electromechanical conversion represented by the displacements generated for a specific actuation movement i at region $\Gamma_{\mathbf{t}_2}^i$ along a specified direction due to an input electrical excitation in the medium (in this study, $\mathbf{E}_1^i$ is prescribed) as described in load case (a) of Figure 3. Its mathematical expression is given by [12]

$$L_2^i(\mathbf{u}_1^i, \phi_1^i) = \int_{\Gamma_{t_2}^i} \mathbf{t}_2^i \mathbf{u}_1^i \, \mathrm{d}\Gamma + \int_{\Gamma_{d_2}^i} d_2^i \phi_1^i \, \mathrm{d}\Gamma = \int_{\Gamma_{t_2}^i} \mathbf{t}_2^i \mathbf{u}_1^i \, \mathrm{d}\Gamma \tag{12}$$

as $d_2^i = 0$ in this problem. Thus, the maximization of output displacement generated in a region $\Gamma_{t_2}^i$ is obtained by maximizing the *mean transduction* quantity ($L_2^i(\mathbf{u}_1^i, \phi_1^i)$). The load cases considered for calculation of *mean transduction* are shown in case (a) of Figure 3.

To provide some stiffness to the multi-flexible structure, the *mean compliance* $L_3^i(\mathbf{u}_3^i, \phi_3^i)$ must also be minimized. The *mean compliance* for each actuation movement i is calculated by considering the load described in case (b) of Figure 3 where a traction $\mathbf{t}_3^i = -\mathbf{t}_2^i$ is applied to region $\Gamma_{\mathbf{t}_2}^i$ and the electric field is kept null inside the medium ($\mathbf{E}_3^i = 0$). Thus, the mean compliance for each actuation movement i is defined by [12]

$$L_3^i(\mathbf{u}_3^i, \phi_3^i) = \int_{\Gamma_{t_2}^i} \mathbf{t}_3^i \mathbf{u}_3^i \, \mathrm{d}\Gamma \tag{13}$$

The *coupling constraint* is obtained by minimizing the absolute value of the corresponding mean transduction $L_4^i(\mathbf{u}_1^i, \phi_1^i)$ between actuated piezoceramic and generated undesired displacements. The *mean transduction* for each actuation movement i is calculated by using Equation (12); however, considering the load case described in case (a) of Figure 3 instead, where traction $\mathbf{t}_4^i$, normal to $\mathbf{t}_2^i$, is applied to region $\Gamma_{\mathbf{t}_2}^i$. Therefore, the *coupling constraint* function for each actuation movement i is given by the following expression [12]:

$$L_4^i(\mathbf{u}_1^i, \phi_1^i) = \int_{\Gamma_{t_4}^i} \mathbf{t}_4^i \mathbf{u}_1^i \, \mathrm{d}\Gamma \tag{14}$$

Finally, a multi-objective function, which combines the above three functions to find an appropriate optimal solution that can incorporate all design requirements for each actuation movement i, is given by

$$\begin{aligned} \mathscr{F}(\rho_1, \rho_2, \rho_3) = {} & w * \ln\left\{ -\frac{1}{\varepsilon_l}\left[\sum_{i=1}^{n} \exp[-\varepsilon_l L_2^i(\mathbf{u}_1^i, \phi_1^i)] \right] \right\} \\ & - \frac{1}{2}(1-w) * \ln\left\{ \sum_{i=1}^{n} \alpha_i (L_3^i(\mathbf{u}_3^i, \phi_3^i))^2 + \sum_{i=1}^{n} \beta_i (L_4^i(\mathbf{u}_1^i, \phi_1^i))^2 \right\} \\ & 0 \leqslant w \leqslant 1, \quad \sum_{i=1}^{n} \alpha_i = 1, \quad \varepsilon_l > 0 \end{aligned} \tag{15}$$

Copyright © 2008 John Wiley & Sons, Ltd.

DOI: 10.1002/nme

where $w, \varepsilon_l, \alpha_i$, and β_i are weight coefficients and n is the number of piezoceramics. In the design of multi-actuated FGM piezoelectric micro-tools, an extra optimization problem of the same type is solved for the piezoceramic domain to find the optimum gradation of the piezoelectric material; however, the optimization problem has the nodal values of $\rho_2(\mathbf{x})$ and element values of $\rho_3(\mathbf{x})$, as design variables. The final optimization problem is defined as follows:

$$
\begin{aligned}
&\text{Maximize:} \quad \mathscr{F}(\rho_1, \rho_2, \rho_3)\\
&\rho_1(\mathbf{x}) \in S, \quad \rho_2(\mathbf{x}) \text{ and } \rho_3(\mathbf{x}) \in S_{\mathrm{PZT}}\\
&\text{subject to:} \quad \mathbf{t}_3^i = -\mathbf{t}_2^i \quad (\Gamma_{\mathbf{t}_3}^i = \Gamma_{\mathbf{t}_2}^i), \quad i = 1 \ldots n\\
&\qquad \mathbf{t}_4^i \cdot \mathbf{t}_2^i = 0 \quad (\Gamma_{\mathbf{t}_4}^i = \Gamma_{\mathbf{t}_2}^i)\\
&\qquad A(\mathbf{u}_1^i, \mathbf{v}_1^i) + B(\phi_1^i, \mathbf{v}_1^i) = L_t(\mathbf{t}_1^i, \mathbf{v}_1^i), \quad B(\varphi_1^i, \mathbf{u}_1^i) - C(\phi_1^i, \varphi_1^i) = L_d(d_1, \varphi_1)\\
&\qquad \text{for } \mathbf{u}_1^i,\ \phi_1^i \in V_a \text{ and } \forall \mathbf{v}_1^i,\ \forall \varphi_1^i \in V_a\\
&\qquad A(\mathbf{u}_3^i, \mathbf{v}_3^i) + B(\phi_3^i, \mathbf{v}_3^i) = L_t(\mathbf{t}_3^i, \mathbf{v}_3^i), \quad B(\varphi_3^i, \mathbf{u}_3^i) - C(\phi_3^i, \varphi_3^i) = L_d(d_3, \varphi_3)\\
&\qquad \text{for } \mathbf{u}_3^i,\ \phi_3^i \in V_c \text{ and } \forall \mathbf{v}_3^i,\ \forall \varphi_3^i \in V_c\\
&\qquad 0 \leqslant \rho_1 \leqslant 1, \quad 0 \leqslant \rho_2 \leqslant 1, \quad 0 \leqslant \rho_3 \leqslant 1\\
&\qquad \Theta_1(\rho) = \int_S \rho_1 \,\mathrm{d}S - \Theta_{1S} \leqslant 0, \quad \Theta_2(\rho) = \int_{S_{\mathrm{PZT}}} \rho_2 \,\mathrm{d}S - \Theta_{2S} \leqslant 0
\end{aligned}
\tag{16}
$$

where

$$
A(\mathbf{u}, \mathbf{v}) = \int_\Omega \boldsymbol{\epsilon}(\mathbf{u})^{\mathrm{t}} \mathbf{C}^{\mathrm{H}} \boldsymbol{\epsilon}(\mathbf{v}) \,\mathrm{d}\Omega, \quad B(\phi, \mathbf{v}) = \int_\Omega (\nabla\phi)^{\mathrm{t}} (\mathbf{e}^{\mathrm{H}})^{\mathrm{t}} \boldsymbol{\epsilon}(\mathbf{v}) \,\mathrm{d}\Omega \tag{17}
$$

$$
C(\phi, \varphi) = \int_\Omega (\nabla\phi)^{\mathrm{t}} \boldsymbol{\varepsilon}^{\mathrm{S}} \nabla\varphi \,\mathrm{d}\Omega, \quad L_t(\mathbf{t}, \mathbf{v}) = \int_{\Gamma_{\mathbf{t}}} \mathbf{t} \cdot \mathbf{v} \,\mathrm{d}\Gamma, \quad L_d(d, \varphi) = \int_{\Gamma_d} \mathrm{d}\varphi \,\mathrm{d}\Gamma \tag{18}
$$

and

$$
\begin{aligned}
V_a &= \{\mathbf{v} = v_i \bar{\mathbf{e}}_i, \varphi \text{ with } \mathbf{v} = 0 \text{ on } \Gamma_u \text{ and } \nabla\varphi = \nabla\varphi_S \text{ in } S_{\mathrm{PZT}},\ i = 1 \text{ or } 3\}\\
V_c &= \{\mathbf{v} = v_i \bar{\mathbf{e}}_i, \varphi \text{ with } \mathbf{v} = 0 \text{ on } \Gamma_u \text{ and } \nabla\varphi = 0 \text{ in } S_{\mathrm{PZT}},\ i = 1 \text{ or } 3\}
\end{aligned}
$$

Note that $B(\phi, \mathbf{v})$ and $C(\phi, \varphi)$ are known. Here S denotes the design domain Ω without including the piezoceramic, Θ_1 is the volume of this design domain, and Θ_{1S} is an upper-bound volume constraint defined to limit the maximum amount of material used to build the coupling structure. Moreover, S_{PZT} denotes the piezoceramic domain, Θ_2 is the constraint related to ρ_2 design variable, and Θ_{2S} is an upper-bound constraint defined to limit ρ_2 values when optimizing the FGM gradation function. The other constraints are equilibrium equations for the piezoelectric medium considering different load cases. The equilibrium equations are solved separately from the optimization problem. They are stated in the problem to indicate that, whatever topology is obtained, it must satisfy the equilibrium equations. The present notation follows closely the one by Bendsøe and Kikuchi [37].

Copyright © 2008 John Wiley & Sons, Ltd.

DOI: 10.1002/nme

4. NUMERICAL IMPLEMENTATION

The continuum distribution of design variables $\rho_1(\mathbf{x})$ and $\rho_2(\mathbf{x})$ are given by the functions [31, 32]

$$\rho_1(\mathbf{x}) = \sum_{I=1}^{n_d} \rho_{1I} N_I(\mathbf{x}), \quad \rho_2(\mathbf{x}) = \sum_{I=1}^{n_d} \rho_{2I} N_I(\mathbf{x}) \tag{19}$$

where ρ_{1I} and ρ_{2I} are nodal design variables, N_I is the finite element shape function that must be selected to provide non-negative values of the design variables, and n_d is the number of nodes at each finite element. The design variables ρ_{1I} and ρ_{2I} can assume different values at each node of the finite element. The additional design variable $\rho_3(\mathbf{x})$ is assumed to be uniform inside each finite element and, in the discretized form, becomes the design variable ρ_{3e}.

Owing to the definition of Equation (19), the material property functions (Equations (10) and (11)) also have a continuum distribution inside the design domain. Thus, considering the mathematical definitions of stiffness and piezoelectric matrices of Equation (5), the material properties must remain inside the integrals and be integrated together by means of the graded finite element concept [29]. The finite element equilibrium equation (8) is solved considering 4-node isoparametric finite elements under either plane stress or plane strain assumption.

When a non-piezoelectric conductor material (usually a metal, such as Aluminum) is considered in Equations (10) and (11), a relevant problem to be solved is how to define the piezoceramic electrodes. If different types of distinct piezoelectric materials are considered, the position of electrodes surface is known and is defined by the piezoceramic domain geometry. However, if a non-piezoelectric conductor material (for example, Aluminum) is also distributed in the piezoceramic design domain, we cannot define '*a priori*' the position of the piezoceramic electrodes because we do not know where the piezoceramic is located in the design domain. To circumvent this problem, we consider the electrical problem independently for each finite element of the piezoceramic domain by defining a pair of electrodes at each finite element, that is, each finite element has its own electrical degrees of freedom as illustrated by Figure 4.

Thus, each finite element has 4 electrical degrees of freedom given by $[\phi_a, \phi_b, \phi_c, \phi_d]$ (nodes are ordered counterclockwise starting from the upper right corner of each finite element) considering

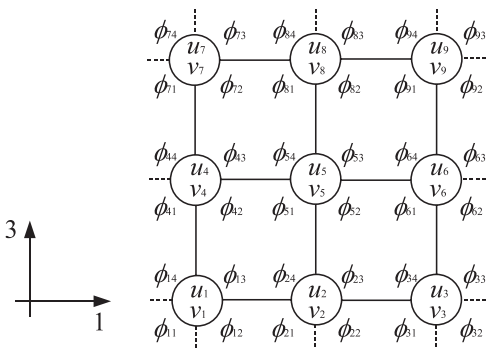

Figure 4. Finite elements with their corresponding electrical degrees of freedom. Here, u_i and v_i denote the node i horizontal and vertical displacement, respectively, and ϕ_{ij} denotes the jth potential at the ith node.

Copyright © 2008 John Wiley & Sons, Ltd.

DOI: 10.1002/nme

that one of the electrodes is grounded. Electrical voltage ϕ_0 is applied to the two upper nodes and thus, the four electrical degrees of freedom are prescribed at each finite element, as follows ($[\phi_0, \phi_0, 0, 0]$) [30]. This is equivalent to applying a constant electrical field along the 3-direction in the design domain (see Figure 4). In this case, all electrical degrees of freedom are prescribed in the FE problem (as already mentioned in Section 2).

By means of the FE matrix formulation, Equation (8), the discrete forms of mean transduction, Equation (12), mean compliance, Equation (13), and the coupling constraint, Equation (14), for the actuation movement i can be calculated numerically through the following expressions:

$$L_2^i(\mathbf{U}_1^i, \mathbf{\Phi}_1^i) = \{\mathbf{U}_1^i\}^{\mathrm{t}}\{\mathbf{F}_2^i\} \tag{20}$$

$$L_3^i(\mathbf{U}_3^i, \mathbf{\Phi}_3^i) = \{\mathbf{U}_3^i\}^{\mathrm{t}}\{\mathbf{F}_3^i\} \tag{21}$$

$$L_4^i(\mathbf{U}_1^i, \mathbf{\Phi}_1^i) = \{\mathbf{U}_1^i\}^{\mathrm{t}}\{\mathbf{F}_4^i\} \tag{22}$$

Note that $\{\mathbf{\Phi}_1^i\}^{\mathrm{t}}\{\mathbf{Q}_2^i\}=0$ (since $\{\mathbf{Q}_2^i\}=0$) and $\{\mathbf{\Phi}_3^i\}^{\mathrm{t}}\{\mathbf{Q}_3^i\}=0$ (since $\{\mathbf{\Phi}_3^i\}=0$). The expression for $L_4^i(\mathbf{U}_1^i, \mathbf{\Phi}_1^i)$ is equal to (20) by substituting $\{\mathbf{F}_2^i\}$ by $\{\mathbf{F}_4^i\}$ and $\{\mathbf{Q}_2^i\}$ by $\{\mathbf{Q}_4^i\}$.

The discretized form of the optimization problem given by Equation (16) is restated as

$$\begin{aligned}
&\text{Maximize:} \quad \mathscr{F}(\rho_{1I}, \rho_{2I}, \rho_{3e}) \\
&\rho_{1I} \in S, \quad \rho_{2I} \text{ and } \rho_{3e} \in S_{\mathrm{PZT}} \\
&\text{subject to:} \quad \{\mathbf{F}_3^i\} = -\{\mathbf{F}_2^i\} \quad (\Gamma_{\mathbf{t}_3}^i = \Gamma_{\mathbf{t}_2}^i), \quad i = 1 \ldots n \\
&\qquad\qquad \{\mathbf{F}_4^i\}^{\mathrm{t}}.\{\mathbf{F}_2^i\} = 0 \quad (\Gamma_{\mathbf{t}_4}^i = \Gamma_{\mathbf{t}_2}^i) \\
&\qquad\qquad [\mathscr{K}_1^i]\{\mathscr{U}_1^i\} = \{\mathscr{Q}_1^i\}, \quad [\mathscr{K}_3^i]\{\mathscr{U}_3^i\} = \{\mathscr{Q}_3^i\} \\
&\qquad\qquad 0 < \rho_{\min} \leqslant \rho_{1I} \leqslant 1, \quad 0 \leqslant \rho_{2J} \leqslant 1, \quad I = 1 \ldots N_e, \quad J = 1 \ldots N_p \\
&\qquad\qquad 0 \leqslant \rho_{3e} \leqslant 1, \quad e = 1 \ldots \mathrm{NE} \\
&\qquad\qquad \sum_{I=1}^{\mathrm{NE}} \int_{S_I} \rho_1 \, \mathrm{d}S_I - \Theta_{1S} \leqslant 0 \\
&\qquad\qquad \sum_{J=1}^{\mathrm{NN}} \int_{S_J} \rho_2 \, \mathrm{d}S_J - \Theta_{2S} \leqslant 0
\end{aligned} \tag{23}$$

where the integrals in the volume constraint expressions are evaluated by using Gauss quadrature (4 points) and considering Equation (19). The parameter N_e is the number of nodes in the non-piezoceramic design domain, and N_p is the number of nodes in the piezoceramic design domain. Moreover, NE and NN denote the number of elements in the piezoceramic and non-piezoceramic design domains, respectively. The matrices $[\mathscr{K}_1^i]$ and $[\mathscr{K}_3^i]$ are reduced forms of the matrix $[\mathscr{K}^i]$ considering non-zero and zero specified voltage degrees of freedom (applied electric field) at the piezoceramic domain, respectively. The initial domain is discretized by finite elements and the design variables (ρ_1, ρ_2, and ρ_3) are the values of ρ_{1I} defined at each finite element node in the non-piezoceramic domain, ρ_{2J} defined at each finite element node, and ρ_{3e} defined at each finite element in the piezoceramic domain. The lower-bound $\rho_{\min}=0.001$ is necessary to avoid numerical problems such as singularity of the stiffness matrix in the finite element formulation

Copyright © 2008 John Wiley & Sons, Ltd.

DOI: 10.1002/nme

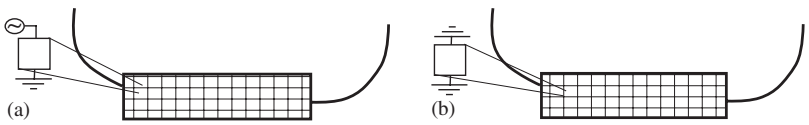

Figure 5. Boundary conditions for the piezoceramic domain: (a) mean transduction and coupling constraint function ($\nabla\phi = \text{constant}$) and (b) mean compliance ($\nabla\phi = 0$).

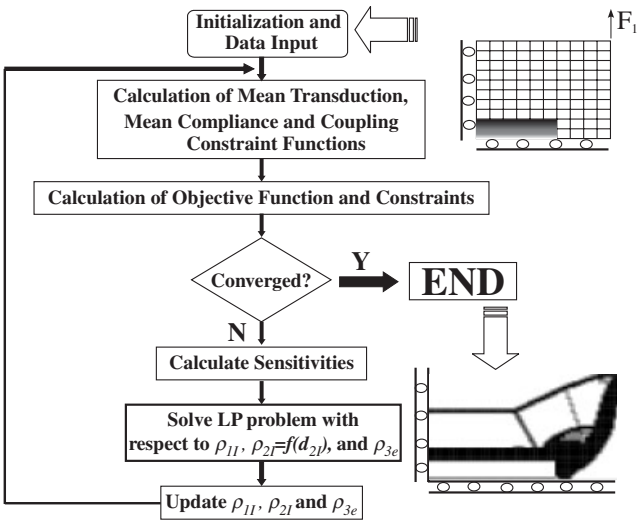

Figure 6. Flowchart of optimization procedure (LP means linear programming).

due to zero stiffness. In practical terms, regions with $\rho_{\min}$ have no structural significance and can be considered void regions.

The boundary conditions for the piezoceramic domain for load cases (a) and (b) of Figure 3 are shown in Figures 5(a) and (b), respectively. They represent constant and null electric field, respectively, applied to the domain.

A flowchart of the optimization algorithm describing the steps involved is shown in Figure 6. The software was implemented using the C language. The mathematical programming method of SLP is applied to solve the optimization problem because there are a large number of design variables and different objective functions and constraints [26, 27, 38]. The linearization of the problem at each iteration requires the sensitivities (gradients) of the multi-objective function and constraints. These sensitivities depend on gradients of mean transduction and mean compliance functions in relation to ρ_{1I}, ρ_{2J}, and ρ_{3e} and are derived in Section 5.

Suitable moving limits are introduced to assure that the design variables do not change by more than 5–15% between consecutive iterations. A new set of design variables ρ_{1I}, ρ_{2J}, and ρ_{3e} are obtained after each iteration, and the optimization continues until convergence is achieved for the objective function. The results are obtained using the continuation method where the penalization coefficient p varies from 1 to 3 along the iterations. The continuation method alleviates the problem of multiple local minima [39]. If the optimization scheme is initiated with large values of

Copyright © 2008 John Wiley & Sons, Ltd.

DOI: 10.1002/nme

penalization coefficient, the continuum problem is close to a discrete problem and, thus, there are many local minima. As a consequence, the optimization method may get trapped in a undesired local minimum. By starting with small values of penalization coefficients, undesired local minima can be avoided, and chances of the algorithm stopping in a more appropriate local minimum are increased. The value of penalization coefficient p_e is equal to 1.0.

5. SENSITIVITY ANALYSIS USING THE ADJOINT METHOD

The gradient of the function $\mathscr{F}$ relative to the design variable A_I (either ρ_{1I}, ρ_{2I}, or ρ_{3e}) is obtained by differentiating (15), and it results in a expression that depends on the sensitivities of mean transduction, mean compliance, and coupling constraint function. These sensitivities have been derived in detail in the study of Carbonari *et al.* [12]. Thus, only changes concerned to the new problem formulation are addressed here.

The mean transduction sensitivity $\partial L_2^i(\mathbf{U}_1^i, \Phi_1^i)/\partial A_I$ considering electrical field excitation is obtained by differentiating Equation (20) and is given by

$$\frac{\partial L_2^i(\mathbf{U}_1^i, \Phi_1^i)}{\partial A_I} = \left\{\frac{\partial \mathbf{U}_1^i}{\partial A_I}\right\}^{\mathrm{t}} \{\mathbf{F}_2^i\} = \{\mathbf{F}_2^i\}^{\mathrm{t}} \left\{\frac{\partial \mathbf{U}_1^i}{\partial A_I}\right\} \tag{24}$$

Note that $\partial \mathbf{F}_2^i/\partial A_I$ is equal to zero as it does not depend on design variables because it is a unit dummy load. The sensitivity $\partial \mathbf{U}_1^i/\partial A_I$ is obtained by differentiating Equation (8), resulting in the following expression:

$$\begin{aligned} [\mathbf{K}_{uu}]\{\mathbf{U}_1^i\} &= \{\mathbf{F}_1^i\} - [\mathbf{K}_{u\phi}]\{\mathbf{\Phi}_1^i\} \\ \Rightarrow [\mathbf{K}_{uu}]\frac{\partial\{\mathbf{U}_1^i\}}{\partial A_I} &= -\frac{\partial[\mathbf{K}_{u\phi}]}{\partial A_I}\{\mathbf{\Phi}_1^i\} - \frac{\partial[\mathbf{K}_{uu}]}{\partial A_I}\{\mathbf{U}_1^i\} \end{aligned} \tag{25}$$

Note that $\partial \mathbf{F}_1^i/\partial A_I = 0$ as it does not depend on design variables because it is an applied load. Moreover, $\partial\{\mathbf{\Phi}_1^i\}/\partial A_I = 0$ because all electrical voltage degrees of freedom are prescribed. Thus,

$$\frac{\partial L_2^i(\mathbf{U}_1^i, \Phi_1^i)}{\partial A_I} = -\{\mathbf{F}_2^i\}^{\mathrm{t}}([\mathbf{K}_{uu}])^{-1}\left\{\frac{\partial[\mathbf{K}_{u\phi}]}{\partial A_I}\{\mathbf{\Phi}_1^i\} + \frac{\partial[\mathbf{K}_{uu}]}{\partial A_I}\{\mathbf{U}_1^i\}\right\} \tag{26}$$

$$= -(\{\mathbf{\Lambda}\}_2^i)^{\mathrm{t}}\left\{\frac{\partial[\mathbf{K}_{u\phi}]}{\partial A_I}\{\mathbf{\Phi}_1^i\} + \frac{\partial[\mathbf{K}_{uu}]}{\partial A_I}\{\mathbf{U}_1^i\}\right\} \quad \text{and} \quad [\mathbf{K}_{uu}]\{\mathbf{\Lambda}\}_2^i = \{\mathbf{F}_2^i\} \tag{27}$$

The sensitivity can be obtained by solving the adjoint problem (27) and substituting $\{\mathbf{\Lambda}\}_2^i$ into (26). Actually, the same expressions are valid for calculating the sensitivity of $L_4^i(\mathbf{U}_1^i, \Phi_1^i)$ by substituting the subscript 2 by 4.

Similarly, the sensitivity of the mean compliance is given by [38]

$$\frac{\partial L_3^i(\mathbf{U}_3^i, \Phi_3^i)}{\partial A_I} = -(\{\mathbf{\Lambda}\}_3^i)^{\mathrm{t}}\left\{\frac{\partial[\mathbf{K}_{u\phi}]}{\partial A_I}\{\mathbf{\Phi}_3^i\} + \frac{\partial[\mathbf{K}_{uu}]}{\partial A_I}\{\mathbf{U}_3^i\}\right\} \quad \text{and} \quad [\mathbf{K}_{uu}]\{\mathbf{\Lambda}\}_3^i = \{\mathbf{F}_3^i\} \tag{28}$$

Copyright © 2008 John Wiley & Sons, Ltd.

DOI: 10.1002/nme

Considering (19), one obtains the derivatives $\partial[\mathbf{K}_{u\phi}]/\partial\rho_{1I}$ and $\partial[\mathbf{K}_{uu}]/\partial\rho_{1I}$, which are given by

$$\begin{aligned}\left[\frac{\partial\mathbf{K}_{uu}}{\partial\rho_{1I}}\right] &= \sum_{e=1}^{\mathrm{NEL}}\int_{\Omega_e}\mathbf{B}_u^{\mathrm{t}}\frac{\partial\mathbf{C}^{\mathrm{H}}}{\partial\rho_1}\frac{\partial\rho_1}{\partial\rho_{1I}}\mathbf{B}_u\,\mathrm{d}\Omega_e \\ &= \sum_{e=1}^{nf}\int_{\Omega_e}\mathbf{B}_u^{\mathrm{t}}\frac{\partial\mathbf{C}^{\mathrm{H}}}{\partial\rho_1}N_I(\mathbf{x})\mathbf{B}_u\,\mathrm{d}\Omega_e \\ \left[\frac{\partial\mathbf{K}_{u\phi}}{\partial\rho_{1I}}\right] &= 0\end{aligned} \tag{29}$$

The derivatives $\partial[\mathbf{K}_{u\phi}]/\partial\rho_{2I}$ and $\partial[\mathbf{K}_{uu}]/\partial\rho_{2I}$ are

$$\begin{aligned}\left[\frac{\partial\mathbf{K}_{uu}}{\partial\rho_{2I}}\right] &= \sum_{e=1}^{\mathrm{NEL}}\int_{\Omega_e}\mathbf{B}_u^{\mathrm{t}}\frac{\partial\mathbf{C}^{\mathrm{H}}}{\partial\rho_2}\frac{\partial\rho_2}{\partial\rho_{1I}}\mathbf{B}_u\,\mathrm{d}\Omega_e \\ &= \sum_{e=1}^{nf}\int_{\Omega_e}\mathbf{B}_u^{\mathrm{t}}\frac{\partial\mathbf{C}^{\mathrm{H}}}{\partial\rho_2}N_I(\mathbf{x})\mathbf{B}_u\,\mathrm{d}\Omega_e \\ \left[\frac{\partial\mathbf{K}_{u\phi}}{\partial\rho_{2I}}\right] &= \sum_{e=1}^{nf}\int_{\Omega_e}\mathbf{B}_u^{\mathrm{t}}\frac{\partial\mathbf{e}^{\mathrm{H}}}{\partial\rho_2}N_I(\mathbf{x})\mathbf{B}_\phi\,\mathrm{d}\Omega_e\end{aligned} \tag{30}$$

and the derivatives $\partial[\mathbf{K}_{u\phi}]/\partial\rho_{3e}$ and $\partial[\mathbf{K}_{uu}]/\partial\rho_{3e}$ are

$$\begin{aligned}\left[\frac{\partial\mathbf{K}_{uu}}{\partial\rho_{3e}}\right] &= 0 \\ \left[\frac{\partial\mathbf{K}_{u\phi}}{\partial\rho_{3e}}\right] &= \int_{\Omega_e}\mathbf{B}_u^{\mathrm{t}}\frac{\partial\mathbf{e}^{\mathrm{H}}}{\partial\rho_{3e}}\mathbf{B}_\phi\,\mathrm{d}\Omega_e\end{aligned} \tag{31}$$

where the definitions of $\mathbf{K}_{uu}$ and $\mathbf{K}_{u\phi}$ were used. The parameter NEL is the total number of finite elements, $\mathbf{B}_u$ is a function of the derivative of shape functions defined in the literature [40], nf is the number of elements connected to node I (that is, the summation is performed considering only these elements), and $\partial\mathbf{C}^{\mathrm{H}}/\partial\rho_1$, $\partial\mathbf{e}^{\mathrm{H}}/\partial\rho_1$, $\partial\mathbf{C}^{\mathrm{H}}/\partial\rho_2$, $\partial\mathbf{e}^{\mathrm{H}}/\partial\rho_2$, and $\partial\mathbf{e}^{\mathrm{H}}/\partial\rho_{3e}$ can be easily obtained by differentiating Equations (9)–(11). In Equation (31), note that only element e depends on the design variable ρ_{3e}.

6. MATERIAL GRADATION CONTROL THROUGH PROJECTION

When designing graded structures, it is important to be able to explicitly control the material gradation. In addition, gradient control is helpful to avoid mesh-dependent solutions. The CAMD approach ensures a continuous material distribution across elements. However, it does not control the local gradient of material distribution. In this study, we introduce a new layer of design variables and use a projection function to obtain material densities at nodes. The implementation of nodal design variables and projection functions [41] is applied on top of the CAMD and leads to explicit

Copyright © 2008 John Wiley & Sons, Ltd.

DOI: 10.1002/nme

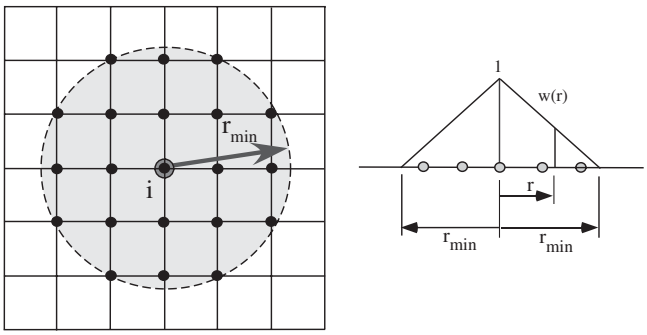

Figure 7. Projection technique using the CAMD concept. Note that $r_{\min}$ is a characteristic length scale, which is independent of mesh discretization.

control of the material gradation. This projection technique is applied only to the design variable ρ_2, which describes the distribution of piezoelectric materials.

Let y_n denote all design variables associated with nodes, and ρ_{2n} denote the values of material density at nodes. Assume that the required change of material density occurs over a minimum length scale denoted by $r_{\min}$. By means of the projection function (f), ρ_{2n} can be obtained from y_n as follows:

$$\rho_{2n} = f(y_n) \tag{32}$$

where f is the projection function defined by

$$\rho_{2i} = f(y_j) = \frac{\sum_{j \in S_i} y_j W(r_{ij})}{\sum_{j \in S_i} W(r_{ij})} \tag{33}$$

and r_{ij} is the distance between nodes j and i, i.e.

$$r_{ij} = \|\mathbf{x}_j - \mathbf{x}_i\| \tag{34}$$

The set of nodes in the domain under influence of node i is denoted as S_i. It consists of a circle of radius $r_{\min}$ centered at node i. The weight function W (defined in Equation (33)) is defined as follows:

$$W(r_{ij}) = \begin{cases} \dfrac{r_{\min} - r_{ij}}{r_{\min}} & \text{if } \mathbf{x}_j \in S_i \\ 0 & \text{otherwise} \end{cases} \tag{35}$$

Figure 7 illustrates the idea of the projection technique. As a consequence, the topology optimization implementation must be revised according to the projection technique [42].

7. EXAMPLES: MULTIFUNCTIONAL AND FUNCTIONALLY GRADED ACTUATORS

The following examples illustrate the design of piezoelectric micro-tools with FGM piezoceramics using the proposed methodology. They consist of regions of piezoceramics whose shape remains

Copyright © 2008 John Wiley & Sons, Ltd.

DOI: 10.1002/nme

Figure 8. Piezoceramic design domain divided into horizontal layers. Design variables ρ_{2J} and ρ_{3e} are defined for each layer interface and each layer, respectively.

Table I. Material properties of piezoceramic (PZT5A) [43].

$\mathbf{c}^{\mathrm{E}}_{11}$ $(10^{10}\,\mathrm{N/m^2})$	12.1	$\mathbf{e}_{13}$ $(\mathrm{C/m^2})$	−5.4
$\mathbf{c}^{\mathrm{E}}_{12}$ $(10^{10}\,\mathrm{N/m^2})$	7.54	$\mathbf{e}_{33}$ $(\mathrm{C/m^2})$	15.8
$\mathbf{c}^{\mathrm{E}}_{13}$ $(10^{10}\,\mathrm{N/m^2})$	7.52	$\mathbf{e}_{15}$ $(\mathrm{C/m^2})$	12.3
$\mathbf{c}^{\mathrm{E}}_{33}$ $(10^{10}\,\mathrm{N/m^2})$	11.1		
$\mathbf{c}^{\mathrm{E}}_{44}$ $(10^{10}\,\mathrm{N/m^2})$	2.30		
$\mathbf{c}^{\mathrm{E}}_{66}$ $(10^{10}\,\mathrm{N/m^2})$	2.10		

unchanged during the optimization, and a domain (S) for the Aluminum frame. The objectives of optimization are to find the optimum material property gradation and polarization sign variation in the piezoceramic domain, and the optimum topology of the flexible structure in the domain S.

The piezoceramic design domain is divided into horizontal layers, and design variables ρ_{2J} and ρ_{3e} are considered for each layer interface and each layer, respectively, as described in Figure 8. All piezoceramic domains are discretized into 20 layers; thus, there are 21 design variables ρ_{2J} and 20 design variables ρ_{3e}. Note that ρ_2 is defined by nodes while ρ_3 is defined by elements (layer). If there are n elements, then there are $(n+1)$ nodes.

Table I presents the piezoelectric material properties used in the simulations for all examples. Here, $\mathbf{c}^{\mathrm{E}}$ and $\mathbf{e}$ denote the elastic and piezoelectric properties of the medium, respectively. Young's modulus and Poisson's ratio of Aluminum are equal to 70 GPa and 0.33, respectively. Two-dimensional isoparametric finite elements under plane-stress assumption are used in the finite element analysis. The following examples are investigated (see Figure 9):

1. single piezoactuator;
2. XY piezoelectric nanopositioner;
3. piezoelectric gripper.

For all examples, unless otherwise specified, the values of ε_l and w coefficients are equal to 10^6 and 0.5, respectively (see the objective function of Equation (15)). The initial values of design variables ρ_{1I} and ρ_{2J} are set equal to 0.25. The penalization coefficient p is continued from 1 to 3 linearly along the iterations. The value of penalization coefficient p_e is equal to 1, which does not change during iterations [33]. The projection technique is applied only for the design variable ρ_2. The value of $r_{\min}$ (see Figure 7) is equal to 0.1 mm (4 elements) for all examples. The volume constraint Θ_{1S} is equal to 25% of the volume of the whole domain Ω without piezoceramic domain. The amount of electric field applied to any of the piezoceramic domains is 400 V/mm.

Copyright © 2008 John Wiley & Sons, Ltd.

DOI: 10.1002/nme

The optimization problem starts in the feasible domain (all constraints satisfied). The results are shown by plotting the average value for design variables ρ_{1I} and ρ_{2J} inside each finite element. The post-processed topology results are obtained by applying a threshold to the value of the ρ_{1I} design variable. This causes a decrease in performance in the piezoactuator design because it may enlarge the stiffness of the coupling structure topology in some cases.

7.1. Single piezoactuator design

The first example illustrates the design of a single-type piezoactuator considering the influence of the FGM piezoceramic material composition and polarization sign. The design domain for this problem with corresponding mechanical and electrical boundary conditions is shown in Figure 9(a). It is discretized with 3600 finite elements and 3721 nodes. The value of the α_1 coefficient (see Equation (15)) is equal to 1.0.

First, the results considering homogeneous piezoceramics are presented for comparison purposes. They are obtained by keeping the piezoceramic domain full of piezoelectric material and out of

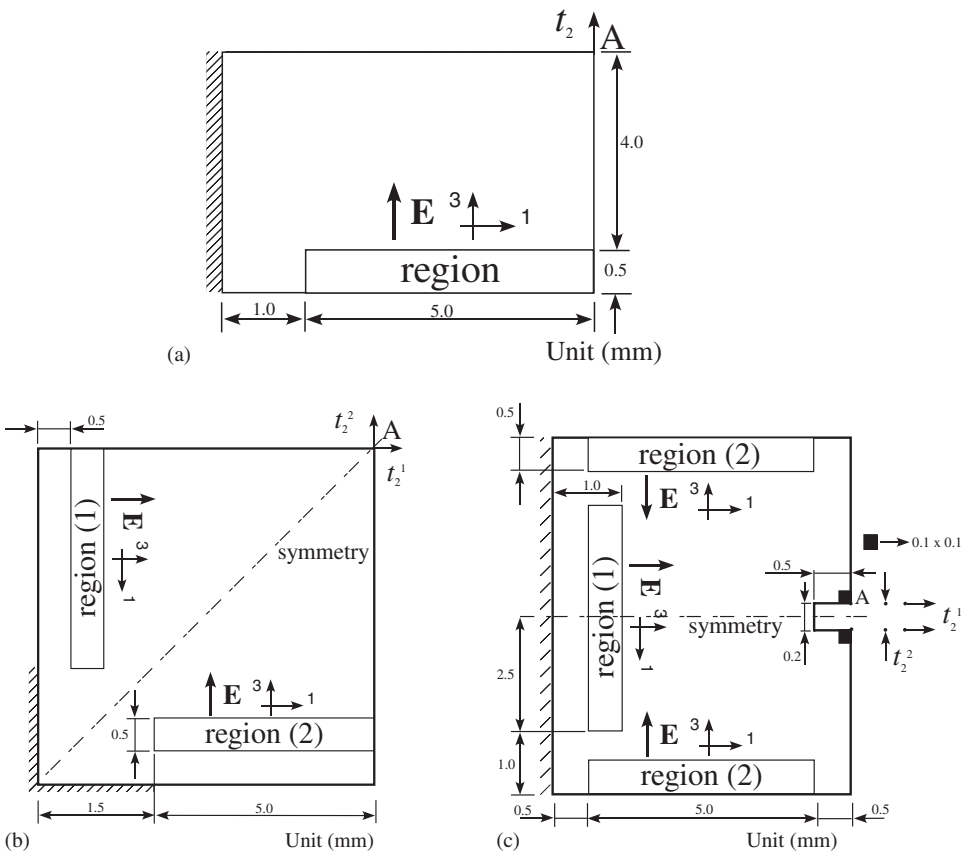

Figure 9. Initial design domains. The piezoceramic design domains are indicated by regions: (a) single piezoactuator; (b) *XY* piezoelectric nanopositioner; and (c) piezoelectric gripper.

Copyright © 2008 John Wiley & Sons, Ltd.

DOI: 10.1002/nme

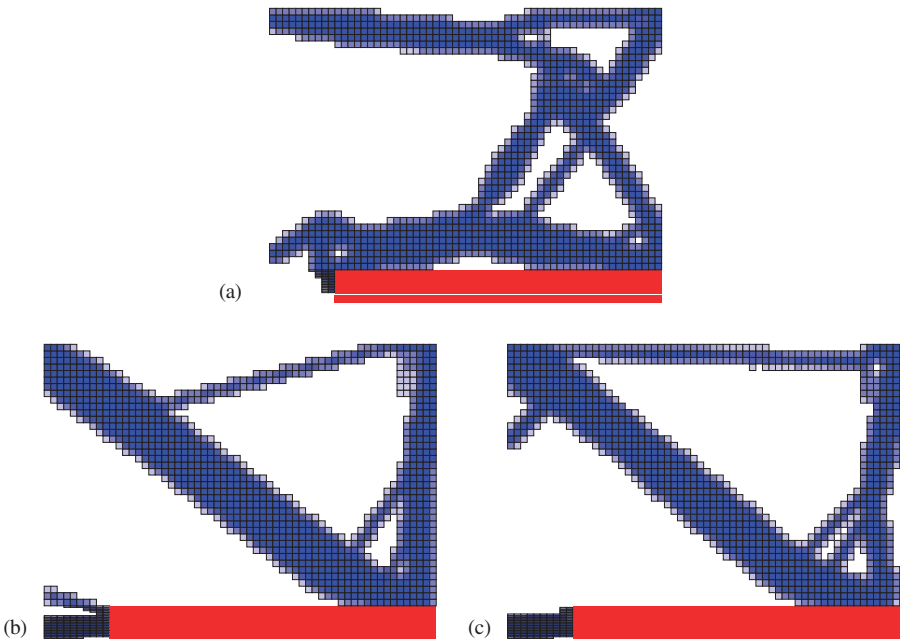

Figure 10. Optimal topology results considering homogeneous piezoceramics: (a) $\rho_{3e}=0.0$ and $\beta_1=0.0$ (or 0.00001); (b) $\rho_{3e}=1.0$ and $\beta_1=0.0$; and (c) $\rho_{3e}=1.0$ and $\beta_1=0.00001$.

the optimization domain. The values of ρ_{3e} are kept fixed and equal to either 0.0 or 1.0. Thus, the corresponding piezoactuator designs obtained considering β_1 coefficients equal to 0.0 or 0.00001 are shown in Figure 10. The result for ρ_{3e} equal to 0.0 and β_1 equal to 0.00001 is quite similar to the result shown in Figure 10(a); thus, it is not explicitly shown. In this case, the magnitude of the coupling ratio β_1 is quite low. The corresponding deformed configuration obtained by using FE of post-processed results are shown in Figure 11.

Table II describes X and Y displacements at point A (u_x and u_y) (see Figure 9(a)) and coupling factors ($R_{yx}=u_x/u_y$) for previous piezoactuator designs considering 400 V/mm electric field applied to the piezoceramic. The largest displacement is obtained for ρ_{3e} equal to 0.0. This performance is probably due to bending deformation of the piezoceramic as shown in Figure 11(a). Such bending deformation is not relevant for the other configurations, as shown in Figures 11(b) and (c). The coupling constraint function reduces the coupling ratio (R_{yx}) as expected, by slightly changing the topologies (see Figures 10(b) and (c)). This tendency will be observed in most of the reported results.

Now the results considering material gradation and change of polarization sign (design variable ρ_{3e}) are presented. In the first results, the material in the piezoceramic domain is allowed to change from piezoelectric to Aluminum. The piezoactuator is designed by specifying a volume constraint of the piezoceramic material Θ_{2S} equal to 50 or 100%. In the latter situation, we allow the optimization method to fill the entire domain with piezoelectric material if necessary.

Initially, the results are obtained by keeping fixed the value of design variable ρ_{3e} in the optimization problem, that is, the polarization sign is not changed. The topology optimization

Copyright © 2008 John Wiley & Sons, Ltd.

DOI: 10.1002/nme

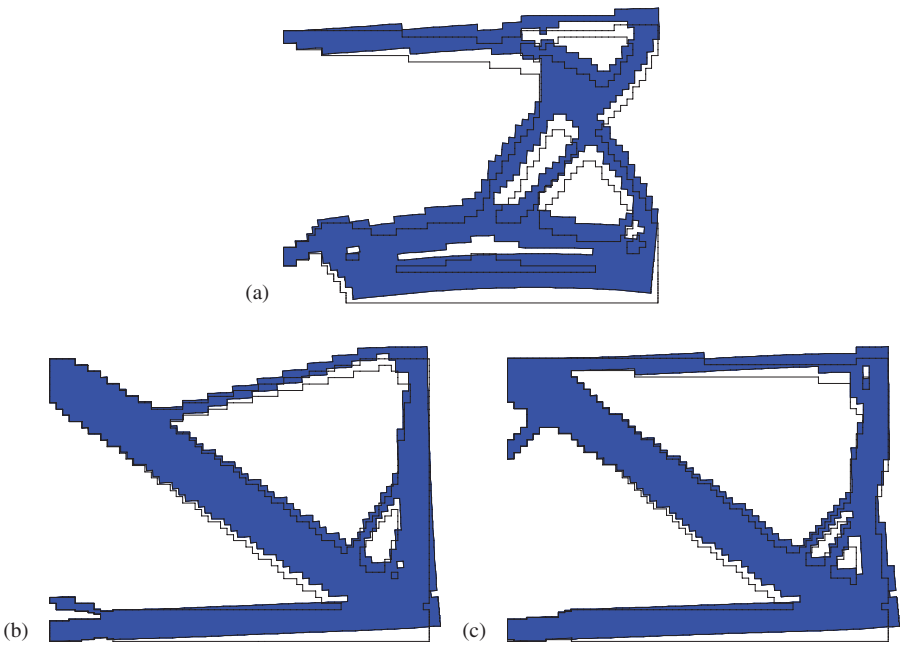

Figure 11. Deformed configurations of post-processed results considering homogeneous piezoceramics: (a) Figure 10(a), $\rho_{3e}=0.0$ and $\beta_1=0.0$ or (0.00001); (b) Figure 10(b), $\rho_{3e}=1.0$ and $\beta_1=0.0$; and (c) Figure 10(c), $\rho_{3e}=1.0$ and $\beta_1=0.00001$.

results obtained by specifying values of Θ_{2S} equal to 50%, ρ_{3e} equal to 0.0 (negative electric field) or 1.0 (positive electric field), and non-zero β_1 coefficients are shown in Figures 12. The corresponding deformed configuration obtained by using FE of post-processed results are shown in Figures 13(a) and (b), respectively. Figures 14(a) and (b), respectively, describe values of ρ_2 along the layer numbers. In all results, Θ_{2S} is active at the end of the optimization. The results obtained specifying Θ_{2S} equal to 100% are not presented because they are quite similar to the homogeneous piezoceramic results of Figure 10. Table II describes generated displacements at point A (u_x and u_y) (see Figure 9(a)) and coupling factors (R_{yx}). For these results (see Figure 12), the largest displacement is also obtained for ρ_{3e} equal to 0.0, even though the bending deformation is also observed in the topology obtained for ρ_{3e} equal to 1.0.

The piezoceramic domain in the design from Figure 12(a) seems to have a natural tendency to bend, as shown in the results of Figure 11(a) considering a homogeneous piezoceramic. However, for Figure 12(b) the bending deformation occurs due to material gradation in the piezoceramic domain. Note that bending deformation was not observed in Figures 11(b) and (c) (homogeneous piezoceramic results). We conclude that an applied electric field corresponding to ρ_{3e} equal to 0.0 gives topology designs with best performance for this example. In addition, from the data presented on Table II, the results for ρ_{3e} equal to 0.0 with material gradation have larger displacements (u_y) and lower coupling ratios than the corresponding homogeneous piezoceramic results (see first line of the table either for 'Topology optimization results' or for 'Post-processed results') however, using only 50% of piezoelectric material. Thus, we conclude that the material gradation can contribute to improve the piezoactuator performance.

Copyright © 2008 John Wiley & Sons, Ltd.

DOI: 10.1002/nme

Table II. Displacements at point A ($E=400\,\mathrm{V/mm}$) and coupling factor ($R_{yx}=u_x/u_y$) for single piezoactuator designs (u_x: undesired displacement).

	Actuators	u_x (nm)	u_y (nm)	$\lvert R_{yx}(\%)\rvert$	Θ_{2S} (%)	ρ_{3e}	β_1
Topology optimization results	Figure 10(a)	6.61	455.44	1.45	—	0.0	0.0
	Figure 10(b)	−83.72	414.11	20.22	—	1.0	0.0
	Figure 10(c)	−1.06	381.72	0.28	—	1.0	10^{-5}
	Figure 12(a)	2.46	554.68	0.44	50	0.0	10^{-4}
	Figure 12(b)	−0.90	321.74	0.28	50	1.0	10^{-5}
	Figure 18(a)	2.17	607.84	0.36	50	0.0	10^{-5}
Post-processed	Figure 11(a)	10.28	442.26	2.32	—	0.0	0.0
	Figure 11(b)	−79.13	406.92	19.45	—	1.0	0.0
	Figure 11(c)	−2.56	372.34	0.69	—	1.0	10^{-5}
	Figure 13(a)	2.54	594.44	0.43	50	0.0	10^{-4}
	Figure 13(b)	−7.82	276.40	2.83	50	1.0	10^{-5}
	Figure 18(b)	−1.64	466.98	0.35	50	1.0	10^{-5}

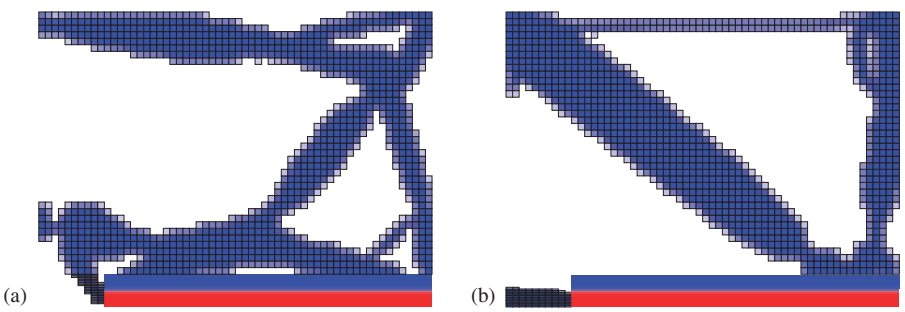

Figure 12. Optimal topology considering distribution of piezoelectric (red) and Aluminum (blue) materials in the piezoceramic domain ($\Theta_{2S}=50\%$): (a) $\rho_{3e}=0.0$ and $\beta_1=0.0001$ and (b) $\rho_{3e}=1.0$ and $\beta_1=0.00001$.

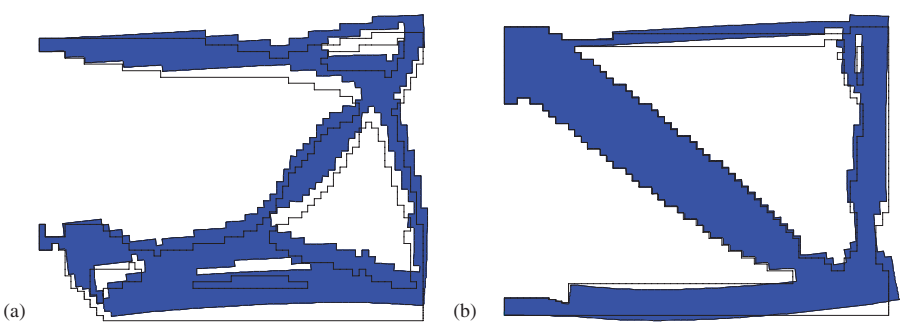

Figure 13. Corresponding FE-deformed configurations of post-processed results: (a) Figure 12(a), $\Theta_{2S}=50\%$, $\rho_{3e}=0.0$, and $\beta_1=0.0001$ and (b) Figure 12(b), $\Theta_{2S}=50\%$, $\rho_{3e}=1.0$, and $\beta_1=0.00001$.

Copyright © 2008 John Wiley & Sons, Ltd.

DOI: 10.1002/nme

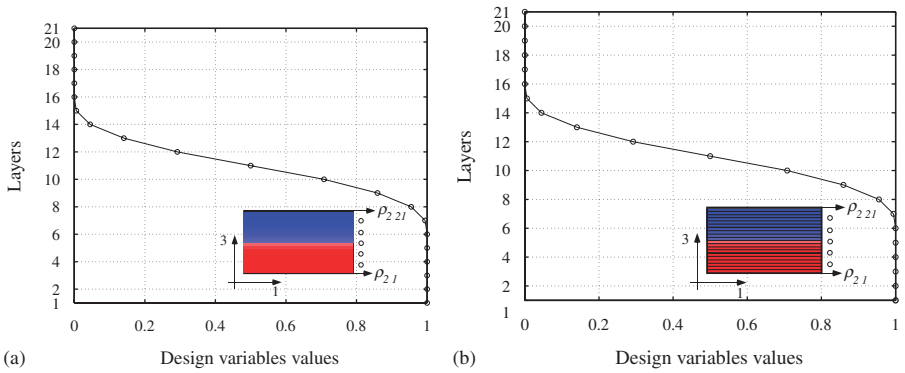

Figure 14. (a) Design variable ρ_2 associated to Figures 12(a) and 13(a) and (b) design variable ρ_2 associated to Figures 12(b) and 13(b).

For the next results the change of the polarization sign is considered in the optimization problem by allowing the value of design variable ρ_{3e} to change. The initial values of design variable ρ_{3e} (ρ_{3e0}) are set equal to 0.1 or 0.9, which implies that the polarization sign starts with a negative or positive value, respectively, in relation to the applied electric field. The topology optimization results obtained by specifying the initial values of ρ_{3e} (ρ_{3e0}) equal to 0.1 or 0.9, Θ_{2S} equal to 50% or 100%, and β_1 coefficient equal to 0.0001 are shown in Figure 15. The corresponding deformed configuration obtained by using FE of post-processed results is shown in Figure 16. Figure 17 describes values of ρ_2 and ρ_3 along the layer numbers.

The coupling structural topologies of results shown in Figures 15(a) and (b) are quite similar, and so are Figures 15(c) and (d). The main difference between both designs is the material gradation in the piezoceramic design domain (see Figures 17(a)–(d)). In all results, Θ_{2S} is active at the end of the optimization. Thus, the results shown in Figures 15(b) and (d) have a homogeneous piezoelectric material in the piezoceramic design domain; however, the polarization sign changes for Figure 15(b). Moreover, Figure 15(d) is quite similar to the homogeneous piezoceramic result (Figure 10(c)).

Table III describes X and Y displacements at point A (u_x and u_y) (see Figure 9(a)) and coupling factors ($R_{yx} = u_x/u_y$) for the piezoactuator designs considering 400 V/mm electric field applied to the piezoceramic.

From Table III, the largest displacements (u_y) are obtained for ρ_{3e0} equal to 0.1 (Figures 15(a) and (b)). This better performance seems to be related to bending deformation caused by a change of the polarization sign (cf. Figures 17(a) and (b)) and material gradation (see, for example, Figure 17(a)), as seen in Figures 16(a) and (b). The displacement values are usually larger than those for the corresponding homogeneous piezoceramic design (see Figure 10(a)), which shows that the change of polarization sign and material gradation contribute to improve performance in piezoactuator design. The deactivation of the coupling constraint function (β_1 coefficient equal to 0.0) does not cause significant changes in the material gradation. This tendency was observed for most results in this paper. The result from Figure 15(b) displays the largest displacement. It does not have material gradation (homogeneous piezoceramic), only change of polarization sign (cf. Figures 17(a) and (b)), which shows that the change of polarization sign seems to be more significant to increase displacement (u_y) than material gradation in this particular example. Thus, for this

Copyright © 2008 John Wiley & Sons, Ltd.

DOI: 10.1002/nme

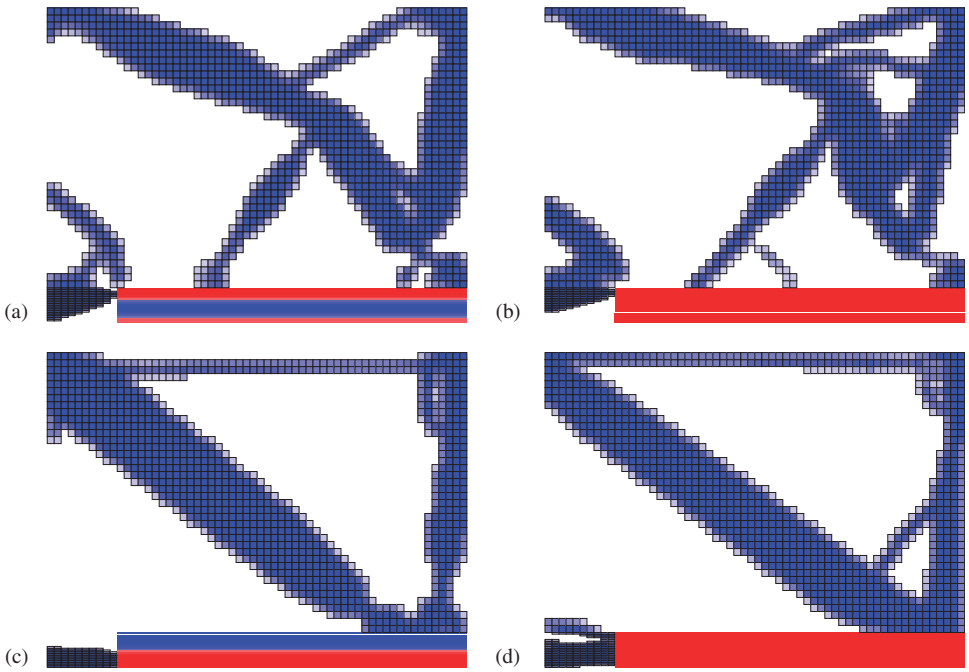

Figure 15. Optimal topology considering distribution of piezoelectric (red) and Aluminum (blue) materials in the piezoceramic domain ($\beta_1 = 0.0001$): (a) $\rho_{3e0} = 0.1$ and $\Theta_{2S} = 50\%$; (b) $\rho_{3e0} = 0.1$ and $\Theta_{2S} = 100\%$; (c) $\rho_{3e0} = 0.9$ and $\Theta_{2S} = 50\%$; and (d) $\rho_{3e0} = 0.9$ and $\Theta_{2S} = 100\%$.

actuator configuration, the FGM piezoceramic design (with a reduced amount of piezoceramic) together with change of polarization sign (Figure 15(a)) generates larger output displacement than the homogeneous piezoceramic design of Figure 10. The change of polarization sign seems to play a more important role to increase the performance (in terms of displacement) of this design than material gradation (cf. either 2nd and 3rd lines of results of Table III or Figures 17(b) with 17(c)).

The bending of the piezoceramic material may generate concern regarding stress levels. However, the present stress levels are relatively low compared with the material strength. The tensile strength of the piezoceramic is about 50 MPa [44]. In general, the highest stress occurs in the Aluminum frame. Another alternative to control the bending stresses consists of pre-stressing the piezoceramic to limit the tensile stresses.

Figures 18 and 19 show results corresponding to those from Figures 12(b) and 15(a), which are obtained without gradation control. The corresponding output displacements are shown in Tables III and II, respectively. We note in these results that the displacement value of post-processed topology ranges from 23.2 to 49.4% of the displacement value of the original topology, respectively. This difference decreases to less than 7% when the material gradation control is applied, which is the case for results from Figures 12(b) and 15(a). This happens probably due to the sharp gradients of material gradation obtained in the piezoceramic domain when a gradation control is not applied. This effect is less pronounced for ρ_{3e} (or ρ_{3e0}) equal to 0.9. Thus, we conclude that the gradation control contributes to reduce the sensitivity of the results to post-processing.

Now, for ρ_{3e0} equal to 0.9 (Figures 15(c) and (d)) the obtained results have smaller output displacements (see Table III) than results obtained for ρ_{3e0} equal to 0.1. Besides, the result from

Copyright © 2008 John Wiley & Sons, Ltd.

DOI: 10.1002/nme

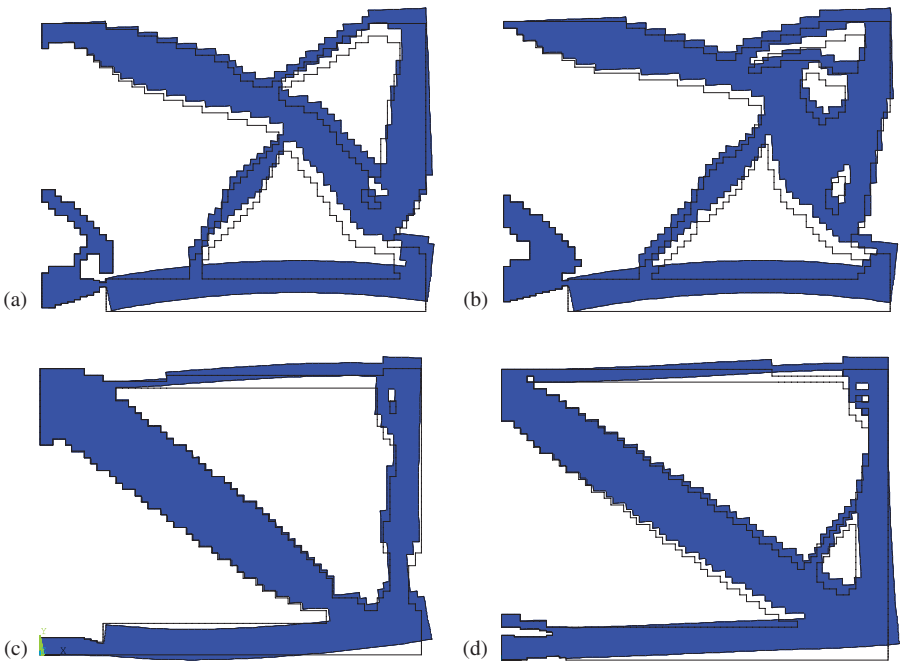

Figure 16. Corresponding FE deformed configurations of post-processed results with $\beta_1 = 0.0001$: (a) Figure 15(a), $\rho_{3e0} = 0.1$ and $\Theta_{2S} = 50\%$; (b) Figure 15(b), $\rho_{3e0} = 0.1$ and $\Theta_{2S} = 100\%$; (c) Figure 15(c), $\rho_{3e0} = 0.9$ and $\Theta_{2S} = 50\%$; and (d) Figure 15(d), $\rho_{3e0} = 0.9$ and $\Theta_{2S} = 100\%$.

Figure 15(d) is quite similar to the homogeneous piezoceramic result shown in Figure 10(b). For this result, there is no significant bending deformation in the piezoceramic domain, as seen in Figure 16(d). Essentially, an elongation of the piezoelectric domain combined with the presence of the coupling structure generates an amplified output displacement at point *A*. The result from Figure 15(c) has a worse performance in terms of output displacement than the homogeneous piezoceramic result (Figure 10(b) or (c)). The coupling structure topology of this result and of homogeneous piezoceramic result (see Figure 10(b) or (c)) is quite similar. The main difference among these designs is the material gradation in the piezoceramic design domain (see Figure 17(c)).

Thus, we conclude that in this design the polarization sign corresponding to ρ_{3e0} equal to 0.9 guides the optimization to a local minimum, which cannot take the advantage of the polarization sign change and material gradation, while the polarization sign corresponding to ρ_{3e0} equal to 0.1 guides the optimization to other local minimum that takes advantage of the polarization sign change and material gradation generating the largest output displacements. Thus, we have shown that in this actuator design the polarization sign must be included as a design variable in the optimization problem to allow the optimization method to explore the advantages of the material gradation in the piezoceramic domain.

In the next result, the material in the piezoceramic domain is allowed to change from piezoelectric material *type 1* to piezoelectric material *type 2*. The property values of piezoelectric material *1* and *2* are given by [24]

$$\mathbf{C}_1 = 4.375 * \mathbf{C}_{\text{Tab1}}, \quad \mathbf{e}_1 = 2.5 * \mathbf{e}_{\text{Tab1}}, \quad \mathbf{C}_2 = 0.1 * \mathbf{C}_{\text{Tab1}}, \quad \mathbf{e}_2 = 0.6 * \mathbf{e}_{\text{Tab1}} \tag{36}$$

Copyright © 2008 John Wiley & Sons, Ltd.

DOI: 10.1002/nme

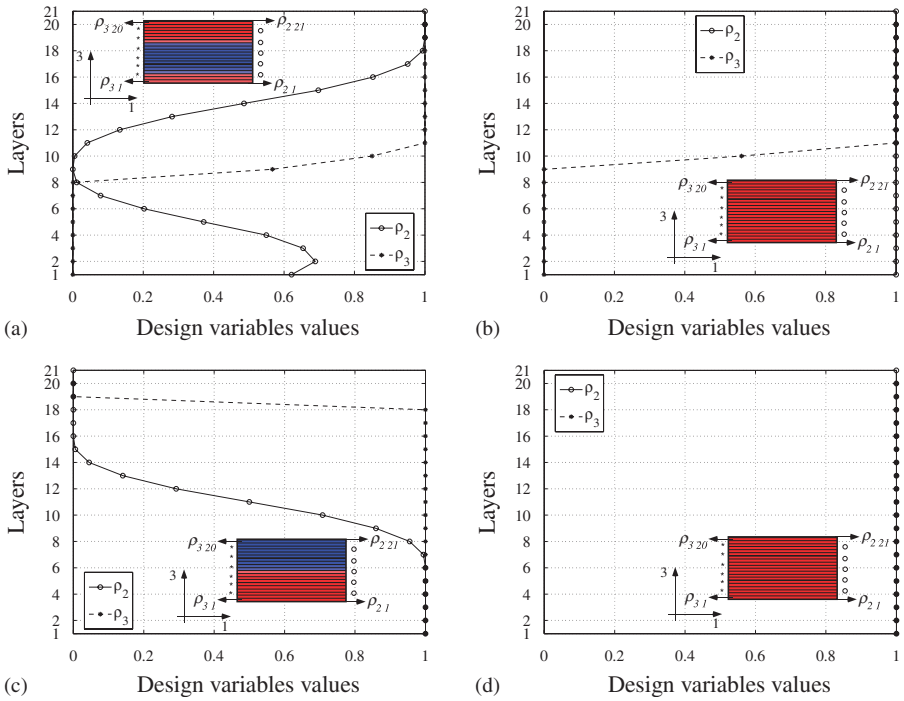

Figure 17. Design variables ρ_2 and ρ_3 values along layer numbers ($\beta_1 = 0.00001$): (a) Figure 15(a), $\rho_{3e0} = 0.1$ and $\Theta_{2S} = 50\%$; (b) Figure 15(b), $\rho_{3e0} = 0.1$ and $\Theta_{2S} = 100\%$; (c) Figure 15(c), $\rho_{3e0} = 0.9$ and $\Theta_{2S} = 50\%$; and (d) Figure 15(d), $\rho_{3e0} = 0.9$ and $\Theta_{2S} = 100\%$.

Table III. Displacements at point A ($E = 400\,\mathrm{V/mm}$) and coupling factor ($R_{yx} = u_x/u_y$) for single piezoactuator designs (u_x: undesired displacement).

Actuators	u_x (nm)	u_y (nm)	$\lvert R_{yx}(\%)\rvert$	Θ_{2S} (%)	ρ_{3e0}	β_1
Figure 15(a)	3.94	676.28	0.58	50	0.1	10^{-4}
Figure 15(b)	−8.71	1048.23	0.83	100	0.1	10^{-4}
Figure 15(c)	−1.27	321.25	0.40	50	0.9	10^{-5}
Figure 15(d)	−0.30	419.83	0.07	100	0.9	10^{-5}
Figure 19(a)	−8.53	655.40	1.30	50	0.1	10^{-5}
Figure 16(a)	4.14	695.93	0.59	50	0.1	10^{-4}
Figure 16(b)	−17.37	947.80	1.83	100	0.1	10^{-4}
Figure 16(c)	−5.97	275.51	2.17	50	0.9	10^{-5}
Figure 16(d)	−2.10	412.32	0.51	100	0.9	10^{-5}
Figure 19(b)	9.64	331.49	2.91	50	0.1	10^{-5}

Copyright © 2008 John Wiley & Sons, Ltd.

DOI: 10.1002/nme

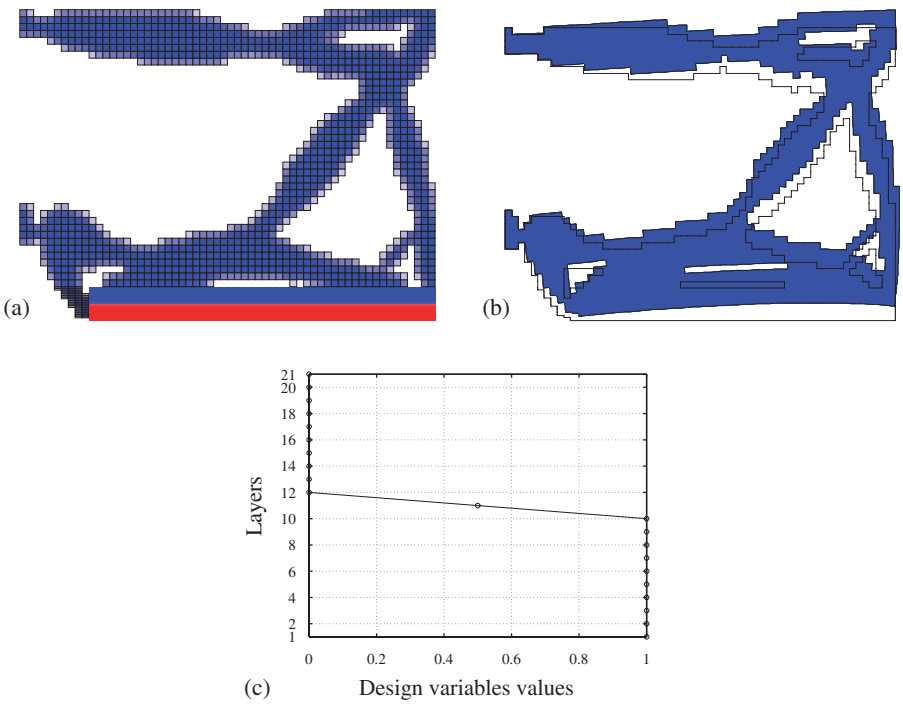

Figure 18. Topology optimization considering distribution of piezoelectric (red) and Aluminum (blue) materials in the piezoceramic domain ($\Theta_{2S} = 50\%$; $\rho_{3e} = 0.0$; $\beta_1 = 0.0001$). No gradation control is applied to the piezoceramic domain: (a) optimal topology; (b) corresponding FE deformed configuration of post-processed result; and (c) design variable ρ_2 along layer numbers.

where $\mathbf{C}_{\text{Tab1}}$ and $\mathbf{e}_{\text{Tab1}}$ are elastic and piezoelectric tensors, respectively, whose property values are described in Table I.

The topology optimization result obtained by specifying β_1 coefficient equal to 10^{-5}, ρ_{3e0} equal to 0.1, and Θ_{2S} equal to 50% is shown in Figure 20(a). The value of ρ_{3e0} equal to 0.1 is chosen based on the conclusion of the previous example. The corresponding deformed configuration obtained by using FE of post-processed results is shown in Figure 20(b). Figure 20(c) describes corresponding values of ρ_2 and ρ_3 along layer numbers. Displacements u_x and u_y at point A (Figure 9(a)) and coupling factors ($R_{yx} = u_x/u_y$) for the piezoactuator designs are described in Table IV.

The piezoactuator shown in Figure 20(a) generates output displacements, which are, up to two times, larger than equivalent homogeneous piezoceramic result (Figure 10(a) or (b)) and with reasonable coupling ratios (see Table IV). This is possible due to a bending deformation of the piezoceramic domain caused by a change of the polarization sign and material gradation (see Figure 20(c)). Thus, we conclude that in this case the presence of the material gradation contributes to improve the output displacement value and coupling ratio and that for this design the polarization sign corresponding to ρ_{3e0} equal to 0.1 guides again the optimization to a local minimum that takes advantage of the bending deformation either due to the polarization sign or material gradation, generating large output displacements and low coupling ratios.

Copyright © 2008 John Wiley & Sons, Ltd.

DOI: 10.1002/nme

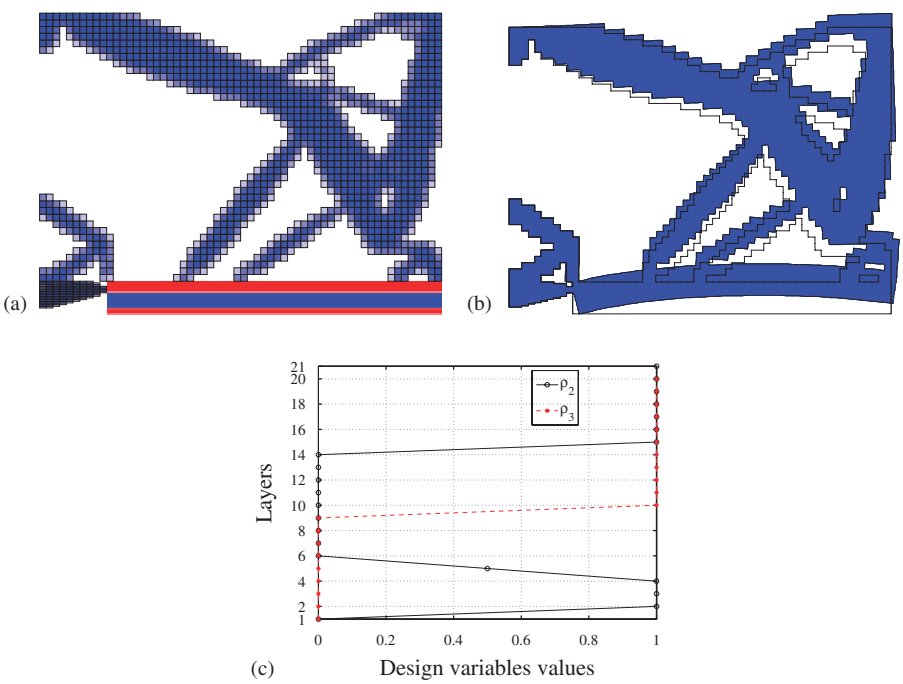

Figure 19. Topology optimization considering distribution of piezoelectric (red) and Aluminum (blue) materials in the piezoceramic domain ($\Theta_{2S}=50\%$; $\rho_{3e0}=0.1$; $\beta_1=0.00001$). No gradation control is applied to the piezoceramic domain: (a) optimal topology; (b) corresponding FE deformed configuration of post-processed result; and (c) ρ_2 and ρ_3 values along layer numbers.

7.2. XY piezoelectric nanopositioner

The design of a planar piezoelectric nanopositioner is considered, and the influence of piezoceramic property gradation and polarization sign variation is assessed. The design domain, together with the mechanical and electrical boundary conditions, is shown in Figure 9(b). The problem is symmetric and has two piezoceramic domains. The FE discretization of the domain consists of 6400 finite elements and 6561 nodes. The values of the α_1 and α_2 coefficients (see Equation (15)) are equal to 0.5. Nanopositioner designs where the material in the piezoceramic domain is allowed to change from piezoelectric to Aluminum are considered.

The *XY* nanopositioner is designed by specifying the volume constraint of piezoceramic material Θ_{2S} equal to 100%. The change of the polarization sign is considered in the optimization problem by allowing the value of design variable ρ_{3e} to change. Figures 21(a) and (b) show topology optimization results obtained by specifying ρ_{3e0} equal to 0.9, and the volume constraint of the piezoceramic material Θ_{2S} equal to 50 or 100%, respectively. The corresponding deformed configuration obtained by means of FE analysis of post-processed results is shown in Figures 22(a) and (b), respectively. Note that there is a slightly change between both topologies (cf. Figures 21(a) and (b)). Figures 23(a) and (b) describe the design variables ρ_2 and ρ_3, respectively, along layer numbers. Table V describes X and Y displacements at point A (u_x and u_y) (see Figure 9(b)) and coupling factors (R_{yx}) considering 400 V/mm electric field applied to the piezoceramic.

Copyright © 2008 John Wiley & Sons, Ltd.

DOI: 10.1002/nme

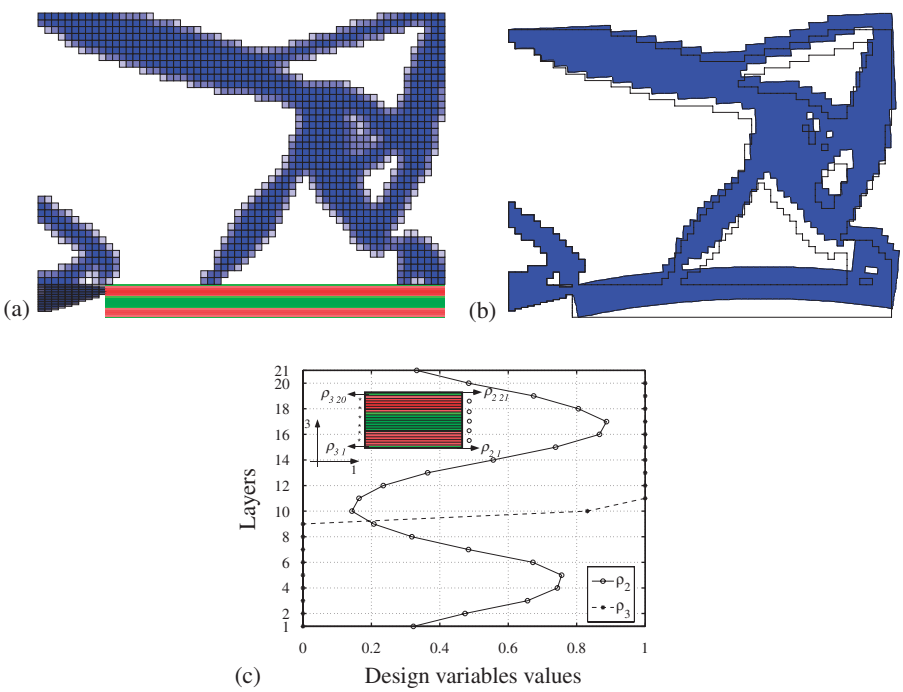

Figure 20. Topology optimization considering the distribution of two types of piezoelectric materials. In the piezoceramic domain, the red and green regions indicate piezoceramic materials type 1 and 2, respectively ($\beta_1 = 10^{-5}$, $\Theta_{2S} = 50\%$, and $\rho_{3e0} = 0.1$): (a) topology optimization result; (b) FE-deformed configuration of post-processed results; and (c) design variables ρ_2 and ρ_3 along layer numbers.

Table IV. Displacements at point A ($E = 400\,\mathrm{V/mm}$) and coupling factor ($R_{yx} = u_x/u_y$) for single piezoactuator designs (u_x: undesired displacement) considering $\beta_1 = 10^{-5}$, $\Theta_{2S} = 50\%$, and $\rho_{3e0} = 0.1$.

	Actuators	u_x (nm)	u_y (nm)	$\lvert R_{yx}\rvert$ (%)
Topology optimization results	Figure 20(a)	−3.70	833.85	0.44
Post-processed topologies	Figure 20(b)	−2.92	581.20	0.50

Note that in Figure 21(b) (Θ_{2S} equal to 100%), the values of ρ_{2J} and ρ_{3e} are equal to 1 (see Figures 22(b) and 23(b)), indicating similarity to a result considering homogeneous piezoceramics. Thus, for comparison purposes, this result is considered as a homogeneous piezoceramic one. Similarly to the previous single piezoactuator results, bending is the dominant deformation mode for the piezoceramic domain; however, the optimization method does not change the polarization sign to improve bending. Thus, for example, in Figure 21(b), where there is no polarization sign change or material gradation, the bending is caused by the mechanical interaction between the piezoceramic domain and the coupling structure. However, in Figures 21(a), it is clear that the material gradation contributes to improve the coupling ratio values, although decreasing the output displacement, as described in Table V. Note that in Figure 21(a), the polarization sign change

Copyright © 2008 John Wiley & Sons, Ltd.

DOI: 10.1002/nme

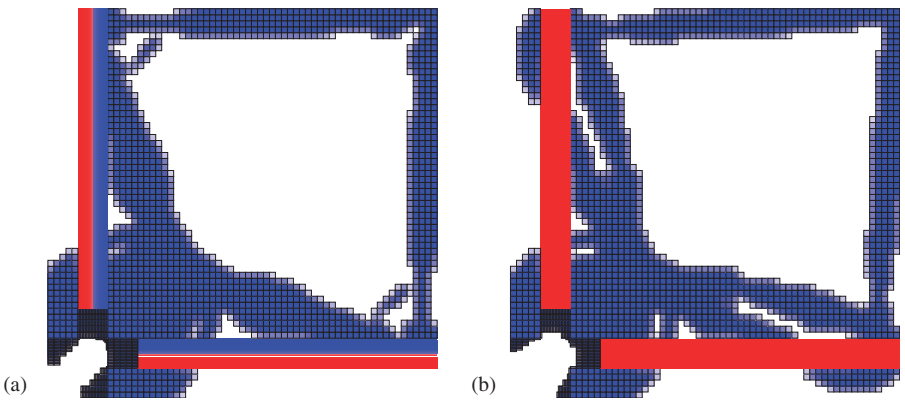

Figure 21. Optimal topology results of *XY* nanopositioners. In the piezoceramic domain, the blue and red regions indicate Aluminum and piezoceramic materials, respectively ($\beta_i = 0.0$ $(i = 1, 2)$): (a) $\rho_{3e0} = 0.9$ and $\Theta_{2S} = 50\%$ and (b) $\rho_{3e0} = 0.9$ and $\Theta_{2S} = 100\%$.

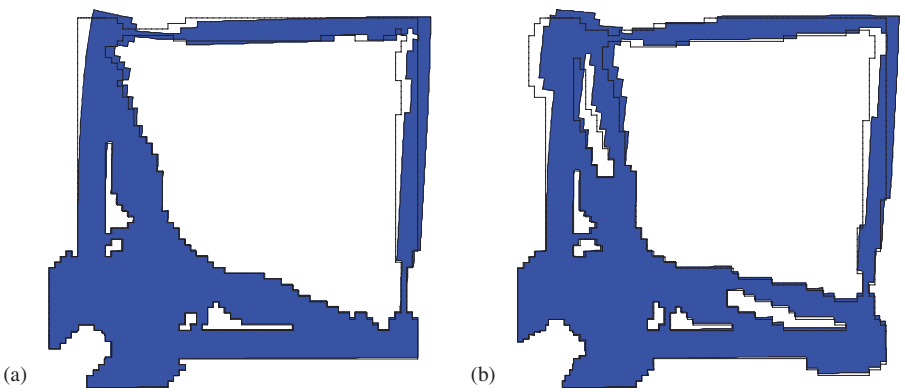

Figure 22. Corresponding FE-deformed configurations of post-processed results: (a) Figure 21(a), $\rho_{3e0} = 0.9$ and $\Theta_{2S} = 50\%$ and (b) Figure 21(b), $\rho_{3e0} = 0.9$ and $\Theta_{2S} = 100\%$.

occurs inside the Aluminum region (see Figure 23(a)); thus, it does not influence the actuator behavior. A slightly smaller displacement and a better (smaller) coupling ratio are obtained when the piezoceramic property gradation variation is considered, however, using only 50% of piezoelectric material. We also note that the results have a small sensitivity to post-processing. The difference between the output displacement of post-processed result and topology optimization result is at most 4%.

The performance for results considering ρ_{3e0} equal to 0.1 is much worse than for results considering ρ_{3e0} equal to 0.9, mainly in terms of coupling ratio. As in the previous example, the reason is that ρ_{3e0} equals to 0.9 guides the optimization to a better local minimum than ρ_{3e0} equals to 0.1, generating almost the same output displacements and much lower coupling ratios. Thus, those results are not shown.

Copyright © 2008 John Wiley & Sons, Ltd.

DOI: 10.1002/nme

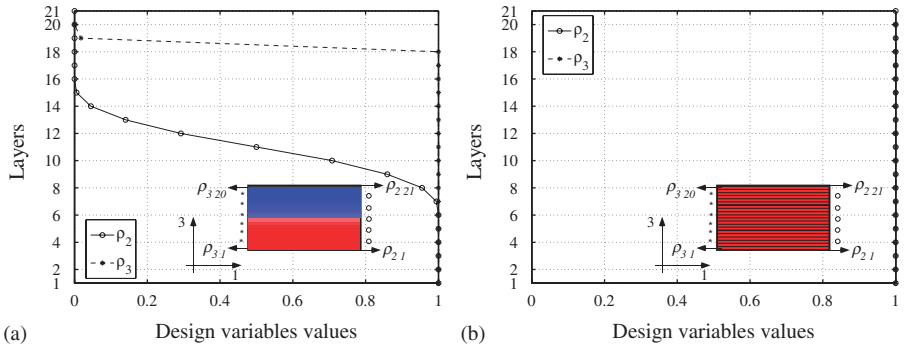

Figure 23. Design variables ρ_2 and ρ_3 along layer numbers: (a) Figure 21(a), $\rho_{3e0}=0.9$ and $\Theta_{2S}=50\%$ and (b) Figure 21(b), $\rho_{3e0}=0.9$ and $\Theta_{2S}=100\%$.

Table V. Displacement at point A ($E=400\,\mathrm{V/mm}$) and coupling factor ($R_{yx}=u_x/u_y$) for XY nanopositioner designs (u_x: undesired displacement) considering $\rho_{3e0}=0.9$ and $\beta_i=0.0$ ($i=1,2$).

	XY nanopositioner	u_y (nm)	u_x (nm)	$\lvert R_{yx}\rvert$ (%)	Θ_{2S} (%)
Topology optimization results	Figure 21(a)	17.21	356.01	4.83	50
	Figure 21(b)	71.88	477.21	15.06	100
Post-processed topologies	Figure 22(a)	24.64	372.86	6.61	50
	Figure 22(b)	77.44	480.18	16.13	100

7.3. Piezoelectric gripper

In the third example, the design of a piezoelectric gripper is considered to show the potential of the method. The design domain for this problem has three piezoceramic domains; however, it is symmetric, as shown in Figure 9(c). The upper and lower piezoceramic regions are responsible for the close and open movements of the jaw. Thus, only the half part of the domain is considered in the design optimization problem, and only two piezoceramic regions are considered. The mechanical and electrical boundary conditions are shown in Figure 9(c). The values of α_1 and α_2 coefficient (see Equation (15)) are equal to 0.5. The material in the piezoceramic domains is allowed to change from piezoelectric to Aluminum. The domain is discretized into 3750 finite elements and 3876 nodes.

The gripper design is obtained by specifying the volume constraint of piezoceramic material Θ_{2S} equal to 100% and by changing the polarization sign (ρ_{3e}) for piezoceramic regions 1 and 2 (see Figure 9(c)). Values of ρ_{3e0} equal to 0.1 are specified for both regions. Figure 24(a) describes the gripper design obtained considering β_i ($i=1,2$) coefficients equal to 0.0, and Figures 24(b)–(e), show corresponding deformed configurations of post-processed results, and graphics of ρ_2 and ρ_3 values along layers for each piezoceramic region, respectively.

Note that a material gradation was obtained for both piezoceramic regions, even though Θ_{2S} is equal to 100%. Among the four possible combinations of polarization signs, the method chose a negative polarization sign for region 1 and a positive polarization sign for region 2 (see Figures 24(d) and (e)). This occurs because the optimization method takes advantage of the bending deformation

Copyright © 2008 John Wiley & Sons, Ltd.

DOI: 10.1002/nme

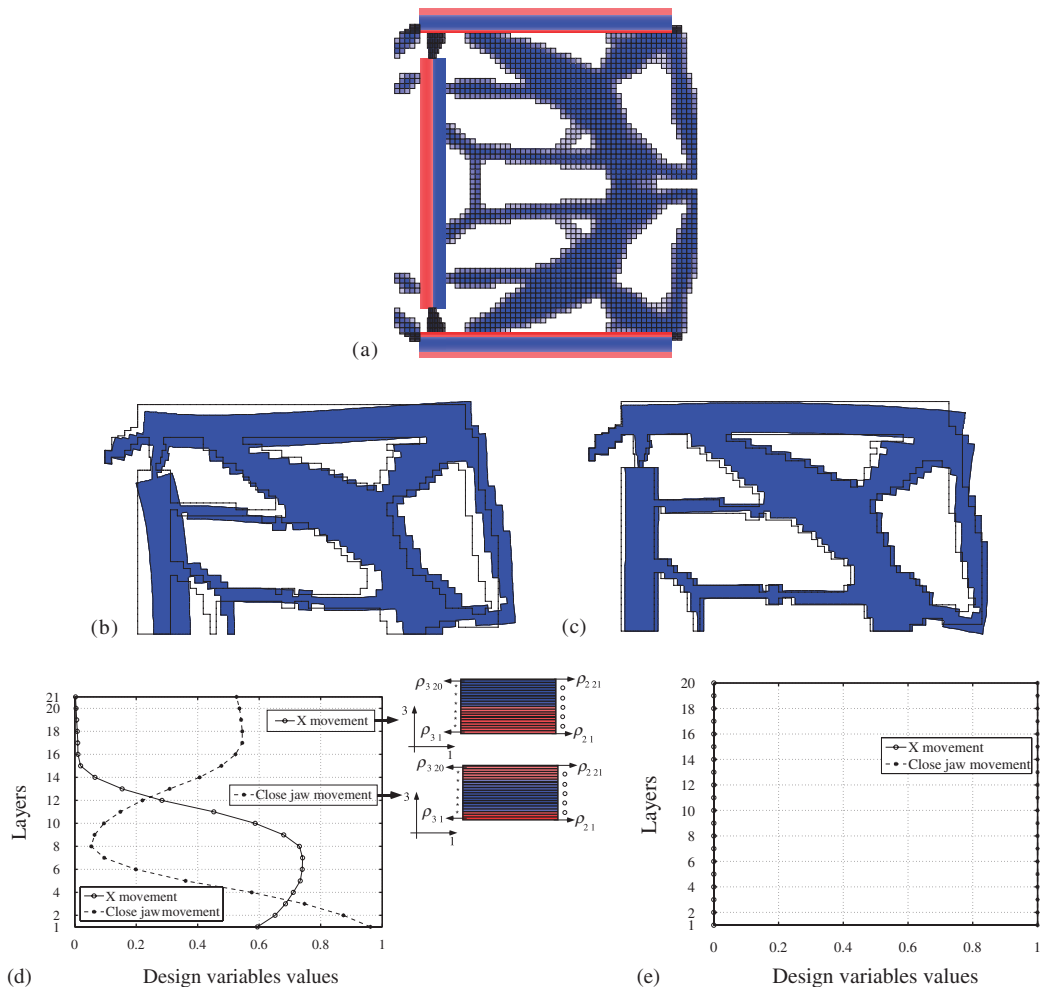

Figure 24. Optimal topology results of piezoelectric gripper considering $\Theta_{2S} = 100\%$, $\beta_i = 0.0$ $(i = 1, 2)$, $\rho_{3e0} = 0.1$ for piezoceramic regions 1 and 2 (see Figure 9(c)): (a) optimal topology; (b) and (c) corresponding FE-deformed symmetric configurations of post-processed topology; (d) design variable ρ_2 along layers for regions 1 and 2; and (e) design variable ρ_3 along layers for regions 1 and 2.

in both regions to maximize the performance, as described in Figure 24(c), which is achieved by defining a material gradation. Table VI describes X and Y displacements at point A (u_x and u_y) (see Figure 9(c)) and coupling factors (R_{yx}) for obtained gripper design considering 400 V/mm electric field applied to the piezoceramic.

A design keeping the polarization sign fixed (design variable ρ_{3e}) was tried; however, it had worse performance than the result that considers material gradation and polarization sign change. Thus, we conclude that in this specific design, material gradation and polarization sign change play an important role to improve actuator performance leading to larger displacements and lower coupling ratios with less amount of piezoelectric material.

Copyright © 2008 John Wiley & Sons, Ltd.

DOI: 10.1002/nme

Table VI. Displacements at point A ($E=400\,\mathrm{V/mm}$), shown in Figure 9(c), and coupling factor ($R_{yx}=u_x/u_y$, $R_{xy}=u_y/u_x$) for gripper design considering $\beta_i=0.0$ and $\Theta_{2S}=100\%$.

	X movement			Closing jaw movement		
Grippers	u_x (nm)	u_y (nm)	$\lvert R_{yx}\rvert$ (%)	u_x (nm)	u_y (nm)	$\lvert R_{xy}\rvert$ (%)
Figure 24(a)	26.71	92.76	28.79	−17.34	104.86	16.54
Figure 24(b)	30.95	109.43	28.28	−5.49	73.13	7.51

8. CONCLUSIONS

The optimized design of FGM piezoactuators including piezoelectric micro-tools actuated by FGM piezoceramics is achieved by means of topology optimization. The FGM piezoactuator performance is obtained by simultaneously optimizing the coupling structural topology, the piezoceramic property gradation, and polarization sign. In the piezoceramic domain, the optimization problem allows the simultaneous distribution of either two piezoelectric materials or a non-piezoelectric (such as Aluminum) and piezoelectric materials. In addition, the polarization sign is also included as a design variable in the optimization problem. The adopted material model is based on the density method. It interpolates fictitious densities at each finite element based on pseudo-densities defined as design variables for each finite element node providing a continuous material distribution in the domain.

The influence of material gradation and change of polarization sign in the actuator performance was verified by means of design examples. We conclude that material gradation plays an important role to improve actuator performance, which may lead to displacements and coupling ratios with reduced amount of piezoelectric material. The change of polarization sign may also have a strong influence in the performance, depending on the design.

The optimization method takes advantage of the bending deformation to improve piezoactuator performance. The bending deformation is obtained either by changing the material gradation or polarization sign or both of them. We note that there is a slight change in the coupling structure topology when comparing the designs considering homogeneous piezoceramics (non-FGM) and FGM piezoceramics.

Extension of this study includes consideration of other performance criteria and other FGM piezoactuators, which can be optimized using the proposed approach. Potentially, this will broaden the range of application of functionally graded piezoelectric actuators in the field of smart structures.

APPENDIX: NOMENCLATURE

List of symbols

$(1,3)$	Cartesian coordinate system
A, B, C	variables
$\mathbf{B}_u, \mathbf{B}_\phi$	functions of the derivative of shape functions
$\mathbf{c}^{\mathrm{E}}$	elastic tensor
$\mathbf{C}^{\mathrm{H}}$	elastic tensor for the mixture

Copyright © 2008 John Wiley & Sons, Ltd.

DOI: 10.1002/nme

$\mathbf{C}_0$	elastic tensor of basic material
$\mathbf{C}_i$	elastic tensor for material type i
d	electrical charge
$\mathbf{D}$	electrical displacement vector
$\mathbf{e}$	piezoelectric tensor
$\overline{\mathbf{e}}_i$	unit vector
$\mathbf{e}^{\mathrm{H}}$	piezoelectric tensor for the mixture
$\mathbf{e}_i$	piezoelectric tensor for material type i
$\mathbf{E}_i^j$	electrical field associated with load case i applied to piezoceramic j
$f(.)$	projection function f
$\mathbf{F}_k^i$	nodal mechanical force for load case k considering piezoceramic i excited
$\mathscr{F}$	objective function
$\mathbf{K}_{uu}$	stiffness matrix
$\mathbf{K}_{u\phi}$	piezoelectric matrix
$\mathbf{K}_{\phi\phi}$	dielectric matrix
$[\mathscr{K}_k^i]$	system matrix for load case k considering piezoceramic i excited
$L_2^i(\mathbf{u}_1^i, \phi_1^i)$	mean transduction
$L_3(\mathbf{u}_3^i, \phi_3^i)$	mean compliance
$L_4^i(\mathbf{u}_1^i, \phi_1^i)$	coupling constraint function
$\mathbf{n}$	normal vector
$N_I(\mathbf{x})$	finite element shape function
N_e	number of nodes in the non-piezoceramic design domain
N_p	number of nodes in the piezoceramic design domain
NEL	total number of finite elements
nf	number of elements connected to node I
NE	number of elements in the piezoceramic design domain
NN	number of elements in the non-piezoceramic design domain
nd	number of nodes at each finite element
n	number of desired output movements
p	penalization factor
$\mathbf{Q}_k^i$	nodal electrical charge for load case k considering piezoceramic i excited
$\{\mathscr{Q}_k^i\}$	force and electrical charge vector for load case k considering piezoceramic i excited
r_{ij}	distance between nodes i and j
$r_{\min}$	minimum length
S	coupling structure design domain
S_{PZT}	piezoceramic design domain
S_i	set of nodes under the influence of node i
$\mathbf{t}$	traction
$\mathbf{T}$	stress tensor
$\mathbf{u}$	displacement field
u_i and v_i	node i horizontal and vertical displacement, respectively
$\mathbf{U}_k^i$	nodal displacements for load case k considering piezoceramic i excited
$\{\mathscr{U}_k^i\}$	displacement and electrical degrees of freedom vector for load case k considering piezoceramic i excited

Copyright © 2008 John Wiley & Sons, Ltd.

DOI: 10.1002/nme

$\mathbf{v}$	virtual displacement
V	space
V_a	space for load case 1
V_b	space for load case 2
V_c	space for load case 3
$\mathbf{x}$	position coordinate vector
y_n	design variable associated with node n
W	general weight coefficient
α_i	weight coefficient for mean compliance
β_i	weight coefficient for coupling constraint function
$\boldsymbol{\varepsilon}^{\mathrm{S}}$	dielectric tensor
ε_l	weight coefficient for mean transduction
$\boldsymbol{\epsilon}(\mathbf{u})$	strain
ϕ	electric potential
φ	virtual electric potential
ϕ_{ij}	jth potential at the ith node
$\phi_a, \phi_b, \phi_c, \phi_d$	electrical degrees of freedom in the finite element
ϕ_0	applied electrical voltage
$\mathbf{\Phi}_k^i$	nodal electric potential vector for load case k considering piezoceramic i excited
$\Gamma_{\mathbf{u}}$	surface of prescribed displacements
Γ_{ϕ}	surface of prescribed electrical degrees of freedom
$\Gamma_{\mathbf{t}_j}^i$	surface of applied mechanical traction for load case j considering piezoceramic i excited
$\Gamma_{d_j}^i$	surface of applied electrical voltage for load case j considering piezoceramic i excited
$\{\mathbf{\Lambda}\}_k^i$	auxiliary vector for load case k considering piezoceramic i excited
Θ_i	volume of design domain i
Θ_{iS}	upper-bound volume constraint for design domain i
ρ_1	design variable to describe the distribution of non-piezoelectric material at each location
ρ_2	design variable to describe the type of piezoelectric material
ρ_3	design variable for the polarization (of the piezoelectric material)
ρ_{iI}	nodal design variable i related to material distribution
ρ_{3e}	element design variable related to polarization sign
ρ_{3e0}	initial value of design variable ρ_{3e}
Ω_e	element domain
Ω	domain
$\nabla\phi$	gradient of electrical potential
∇	gradient operator

ACKNOWLEDGEMENTS

The first author thanks CNPq (Conselho Nacional de Desenvolvimento Científico e Tecnológico-Brazil), for supporting him through a doctoral fellowship (no. 140687/2003-3). The second author thanks FAPESP

Copyright © 2008 John Wiley & Sons, Ltd.

DOI: 10.1002/nme

(Fundação de Amparo à Pesquisa do Estado de São Paulo), CNPq, and the University of Illinois at Urbana-Champaign (UIUC) for inviting him as a Visiting Professor during the Summer/2006. The third author thanks FAPESP for the Visiting Scientist award at USP (University of São Paulo) through project number 2008/5070-0. We gratefully acknowledge the U.S.A. NSF through the project CMS#0303492 (Inter-Americas Collaboration in Materials Research and Education, PI Prof. W. Soboyejo, Princeton University).

REFERENCES

1. Ishihara H, Arai F, Fukuda T. Micro mechatronics and micro actuators. *IEEE/ASME Transactions on Mechatronics* 1996; **1**(1):68–79.
2. Indermuhle PF, Jaecklin V, Brugger J, Linder C, Rooij ND, Binggeli M. AFM imaging with an xy—micropositioner with integrated tip. *Sensors and Actuators A*: *Physical* 1995; **47**(1–3):562–565.
3. Ku S, Pinsopon U, Cetinkunt S, Nakajima S. Design, fabrication, and real-time neural network control of a three-degrees-of-freedom nanopositioner. *IEEE/ASME Transactions on Mechatronics* 2000; **5**(3):273–279.
4. Chang S, Tseng C, Chien H. An ultra-precision $xy\theta_z$ piezo-micropositioner, part I: design and analysis. *IEEE Transactions on Ultrasonics*, *Ferroelectrics*, *and Frequency Control* 1999; **46**(4):897–905.
5. Ferreira A, Agnus J, Chaillet N, Breguet JM. A smart microrobot on chip: design, identification, and control. *IEEE/ASME Transactions on Mechatronics* 2004; **9**(3):508–519.
6. Pérez R, Agnus J, Clévy C, Hubert A, Chaillet N. Modeling, fabrication, and validation of a high-performance 2-DOF piezoactuator for micromanipulation. *IEEE/ASME Transactions on Mechatronics* 2005; **10**:161–171.
7. Menciassi A, Eisinberg A, Carrozza MC, Dario P. Force sensing microinstrument for measuring tissue properties and pulse in microsurgery. *IEEE/ASME Transactions on Mechatronics* 2003; **8**(1):10–17.
8. Claeyssen F, Le Letty R, Barillot F, Lhermet N, Fabbro H, Guay P, Yorck M, Bouchilloux P. Mechanisms based on piezo actuators. *Proceedings on Industrial and Commercial Applications of Smart Structures Technologies of Eighth SPIE* (*Annual International Symposium on Smart Structures and Materials*), vol. 4332, Newport Beach, CA, 2001; 225–233.
9. Howell LL. *Compliant Mechanisms*. Wiley: New York, U.S.A., 2001.
10. Canfield S, Frecker MI. Topology optimization of compliant mechanical amplifiers for piezoelectric actuators. *Structural and Multidisciplinary Optimization* 2000; **20**:269–279.
11. Frecker M. Recent advances in optimization of smart structures and actuators. *Journal of Intelligent Material Systems and Structures* 2003; **14**(5):207–216.
12. Carbonari RC, Silva ECN, Nishiwaki S. Design of piezoelectric multiactuated microtools using topology optimization. *Smart Materials and Structures* 2005; **14**(6):1431–1447.
13. Suresh S, Mortensen A. *Fundamentals of Functionally Graded Materials*. IOM Communications Ltd.: London, England, 1988.
14. Miyamoto Y, Kaysser WA, Rabin BH, Kawasaki A, Ford RG. *Functionally Graded Materials*: *Design*, *Processing and Applications*. Kluwer: Dordrecht, 1999.
15. Paulino GH, Jin ZH, Dodds Jr RH. Failure of functionally graded materials. In *Comprehensive Structural Integrity*, vol. 2, Karihaloo B, Knauss WG (eds). Elsevier Science: 2003; 607–644.
16. Sigmund O. Topology optimization: a tool for the tailoring of structures and materials. *Philosophical Transactions of the Royal Society*: *Science into the Next Millennium* (*Issue III*, *Mathematics*, *Physics and Engineering*, *Special Issue*) 2000; **358**(1765):211–227.
17. Torquato S. *Random Heterogeneous Materials—Microstructure and Macroscopic Properties*. Springer: New York, U.S.A., 2002.
18. Bendsøe MP, Sigmund O. *Topology Optimization—Theory*, *Methods and Applications*. Springer: New York, U.S.A., 2003.
19. Cho JR, Choi JH. A yield-criteria tailoring of the volume fraction in metal-ceramic functionally graded material. *European Journal of Mechanics A—Solids* 2004; **23**(2):271–281.
20. Turteltaub S. Optimal material properties for transient problems. *Structural and Multidisciplinary Optimization* 2001; **22**:157–166.
21. Turteltaub S. Optimal control and optimization of functionally graded materials for thermomechanical processes. *International Journal of Solids and Structures* 2002; **39**:3175–3197.
22. Turteltaub S. Functionally graded materials for prescribed field evolution. *Computer Methods in Applied Mechanics and Engineering* 2002; **191**:2283–2296.

Copyright © 2008 John Wiley & Sons, Ltd.

DOI: 10.1002/nme

23. Paulino GH, Silva ECN. Design of functionally graded structures using topology optimization. *Materials Science Forum* 2005; **492–493**:435–440.
24. Almajid A, Taya M, Hudnut S. Analysis of out-of-plane displacement and stress field in a piezocomposite plate with functionally graded microstructure. *International Journal of Solids and Structures* 2001; **38**(19):3377–3391.
25. Zhifei S. General solution of a density functionally gradient piezoelectric cantilever and its applications. *Smart Materials and Structures* 2002; **11**:122–129.
26. Vanderplaatz GN. *Numerical Optimization Techniques for Engineering Design*: *With Applications*. McGraw-Hill: New York, U.S.A., 1984.
27. Hanson R, Hiebert K. A sparse linear programming subprogram. *Technical Report SAND81-0297*, Sandia National Laboratories, 1981.
28. Lerch R. Simulation of piezoelectric devices by two-and three-dimensional finite elements. *IEEE Transactions on Ultrasonics*, *Ferroelectrics and Frequency Control* 1990; **37**(2):233–247.
29. Kim JH, Paulino GH. Isoparametric graded finite elements for nonhomogeneous isotropic and orthotropic materials. *Journal of Applied Mechanics* (ASME) 2002; **69**(4):502–514.
30. Buehler MJ, Bettig B, Parker GG. Topology optimization of smart structures using a homogenization approach. *Journal of Intelligent Material Systems and Structures* 2004; **15**(8):655–667.
31. Matsui K, Terada K. Continuous approximation of material distribution for topology optimization. *International Journal for Numerical Methods in Engineering* 2004; **59**(14):1925–1944.
32. Rahmatalla S, Swan CC. A Q4/Q4 continuum structural topology optimization implementation. *Structural and Multidisciplinary Optimization* 2004; **27**:130–135.
33. Kögl M, Silva ECN. Topology optimization of smart structures: design of piezoelectric plate and shell actuators. *Smart Materials and Structures* 2005; **14**(2):387–399.
34. Carbonari RC, Nishiwaki S, Paulino GH, Silva ECN. Piezoactuator design considering the optimum placement of FGM piezoelectric material. *Proceedings on Modeling*, *Signal Processing*, *and Control for Smart Structures of 14th SPIE* (*Annual International Symposium on Smart Structures and Materials*), vol. 6523, San Diego, CA, 2007; C65230C-1–C65230C-12. DOI: 10.1117/12.715411.
35. Carbonari RC, Silva ECN, Nishiwaki S. Optimum placement of piezoelectric material in piezoactuator design. *Smart Materials and Structures* 2007; **16**(1):207–220.
36. Nishiwaki S, Min S, Yoo J, Kikuchi N. Optimal structural design considering flexibility. *Computer Methods in Applied Mechanics and Engineering* 2001; **190**:4457–4504.
37. Bendsøe MP, Kikuchi N. Generating optimal topologies in structural design using a homogenization method. *Computer Methods in Applied Mechanics and Engineering* 1988; **71**:197–224.
38. Silva ECN, Nishiwaki S, Kikuchi N. Topology optimization design of flextensional actuators. *IEEE Transactions on Ultrasonics*, *Ferroelectrics and Frequency Control* 2000; **47**(3):657–671.
39. Stolpe M, Svanberg K. On the trajectories of penalization methods for topology optimization. *Structural and Multidisciplinary Optimization* 2001; **21**:128–139.
40. Cook RD, Malkus DS, Plesha ME. *Concepts and Applications of Finite Element Analysis*. Wiley: New York, U.S.A., 1989.
41. Guest JK, Prévost JH, Belytschko T. Achieving minimum length scale in topology optimization using nodal design variables and projection functions. *International Journal for Numerical Methods in Engineering* 2004; **61**:238–254.
42. Paulino GH, Silva ECN, Le CH. Optimal design of periodic functionally graded composites with prescribed properties. *Structural and Multidisciplinary Optimization* 2008; DOI: 10.1007/s00158-008-0300-1.
43. Ikeda T. *Fundamentals of Piezoelectricity*. Oxford University Press: Oxford, 1996.
44. Fett T, Munz D, Thun G. Tensile and bending strength of piezoelectric ceramics. *Journal of Materials Science Letters* 1999; **18**:1899–1902.

Copyright © 2008 John Wiley & Sons, Ltd.